Development 127, 1767-1787 (2000)
Printed in Great Britain © The Company of Biologists Limited 2000
DEV7765

Microtubules and mitotic cycle phase modulate spatiotemporal distributions of F-actin and myosin II in *Drosophila* syncytial blastoderm embryos.

Victoria E. Foe[1,*], Christine M. Field[2] and Garrett M. Odell[1]

[1]Department of Zoology, University of Washington, Seattle WA 98195-1800, USA
[2]Harvard Medical School, 240 Longwood Avenue, Boston MA 02115-5731, USA
*Author for correspondence (e-mail: vicfoe@zoology.washington.edu)

Accepted 31 January; published on WWW 6 April 2000

SUMMARY

We studied cyclic reorganizations of filamentous actin, myosin II and microtubules in syncytial *Drosophila* blastoderms using drug treatments, time-lapse movies and laser scanning confocal microscopy of fixed stained embryos (including multiprobe three-dimensional reconstructions). Our observations imply interactions between microtubules and the actomyosin cytoskeleton. They provide evidence that filamentous actin and cytoplasmic myosin II are transported along microtubules towards microtubule plus ends, with actin and myosin exhibiting different affinities for the cell's cortex. Our studies further reveal that cell cycle phase modulates the amounts of both polymerized actin and myosin II associated with the cortex. We analogize pseudocleavage furrow formation in the *Drosophila* blastoderm with how the mitotic apparatus positions the cleavage furrow for standard cytokinesis, and relate our findings to polar relaxation/global contraction mechanisms for furrow formation.

Movies available on-line:
http://www.biologists.com/Development/movies/dev7765.html
http://raven.zoology.washington.edu/downTheTubes/

Key words: Microtubule, Myosin II, F-actin, Kinesin-like protein, Cytoskeletal interaction, Polar relaxation, Contractile ring, Cytokinesis, Pseudocleavage furrow, *Drosophila*, Three-dimensional reconstruction

INTRODUCTION

Many processes critical for development suggest interactions (of unknown cause) between microtubules, actin and myosin. These include (1) directed lamellipodial protrusion in crawling cells (e.g. Waterman-Storer and Salmon, 1999; Waterman-Storer et al., 1999), (2) sperm-entry-activated, colcemid-sensitive, rotation of the cortex relative to the deep cytoplasm in amphibian eggs, establishing the dorsoventral body axis of the embryo (Larabell et al., 1996; Vincent and Gerhart, 1987), and (3) during cytokinesis, cortical flow away from spindle poles (Cao and Wang, 1990b; Dan, 1954; Fishkind et al., 1996; Wang et al., 1994) and cytoplasmic myosin movement towards the spindle mid-zone (Yumura and Uyeda, 1997a), movements that are oriented by mitotic apparatus position.

In early *Drosophila* embryogenesis, three large-scale morphogenetic events also suggest interactions between the actomyosin cytoskeleton and microtubule arrays: (1) the stepwise migration of nuclei through the syncytial egg's interior towards the cortex in phase with cycles of microtubule and F-actin reorganization (Baker et al., 1993; von Dassow and Schubiger, 1994; Zalokar and Erk, 1976), (2) cycles of 'bud' and 'pseudocleavage furrow' formation after migrating nuclei reach the cortex of the still syncytial embryo (Foe and Alberts, 1983), which we focus on in this study, and (3) cellularization, the actin, myosin and microtubule-requiring process which partitions the syncytial cytoplasm into mononucleate cells (reviewed in Foe et al., 1993; Schejter and Wieschaus, 1993). Several proteins essential for contractile ring formation during cytokinesis – the septin protein Peanut (Neufeld and Rubin, 1994), Diaphanous (Castrillon and Wasserman, 1994) and Anillin (C. M. F., unpublished data) – are also implicated in pseudocleavage furrow formation in *Drosophila* (Afshar et al., 1999; Field and Alberts, 1995; Miller and Kiehart, 1995; Rothwell et al., 1998). This suggests that studies of bud/pseudocleavage furrow formation will provide insights relevant to cytokinesis.

We observe temporal and spatial changes in the organization of filamentous actin (F-actin hereafter), conventional non-muscle myosin (myosin II hereafter), centrosomes and microtubules in the *Drosophila* syncytial blastoderm correlated with mitotic cycle phase, and report drug experiments to probe for interactions between the cytoskeletal elements. Our evidence implicates oriented arrays of microtubules in causing rapid spatial reorganizations of myosin II and F-actin in synchrony with the mitotic cycle. These spatial reorganizations occur against a background of embryo-wide, large-amplitude, temporal oscillations in the fraction of actin polymerized and concentrated at the cortex, and in the fraction of myosin II concentrated at the embryo's cortex (as detected by two different polyclonal antibodies). These embryo-wide oscillations, interesting in their own right, complicate

understanding how microtubules may affect F-actin and myosin II spatial patterning. Fortunately, in early *Drosophila* development, cell cycle-related changes in the cortex that depend on microtubules can be distinguished from those that do not. Before their 10th division cycle, nuclei with associated microtubule arrays undergo replication and movement cycles in the embryo's interior without contacting the cortex (Foe and Alberts, 1983; Zalokar and Erk, 1976). Before cycle 10, we can therefore observe microtubule-independent kinematics of cortical F-actin and myosin II. Migrating nuclei reach the cortex during early interphase of cycle 10 (Foe and Alberts, 1983); thereafter their associated microtubule arrays do affect cortical F-actin (Karr and Alberts, 1986; Kellogg et al., 1988; Warn et al., 1984)and myosin II reorganizations . Rapid cycles of cytoskeletal reorganization near the cortex correlate with the formation during interphase of 'buds' – cytoplasmic protrusions each containing one nucleus – and bud collapse during anaphase (Foe and Alberts, 1983). A time-lapse video of bud kinematics is available at http://raven.zoology.washington.edu/downTheTubes/. Bud formation cycles require the presence at the cortex of centrosomes and the microtubules they nucleate, but not necessarily of nuclei (Raff and Glover, 1988; Yasuda et al., 1991). The 'trenches' between buds, called pseudocleavage furrows (or metaphase furrows) are shallow during cycle 10, but invaginate deep enough in later cycles to isolate adjacent nuclei. Functionally, this isolation of syncytial nuclei prevents chromosome capture by microtubules emanating from centrosomes of adjacent nuclei (Postner et al., 1992; Sullivan et al., 1990). We focus on the cytoskeletal dynamics cyclically producing cytoplasmic buds and pseudocleavage furrows between buds, two features of the same underlying phenomenon.

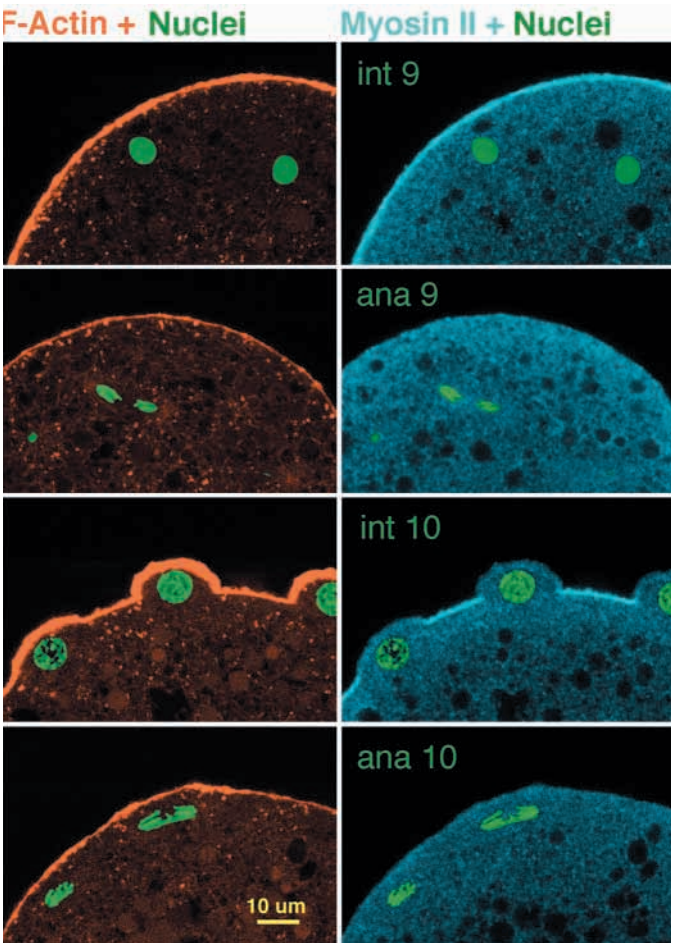

Fig. 1. Cross-sectional LSCM images of the *Drosophila* embryo anterior showing F-actin (red), myosin II (blue) and nuclei (green) during cycle 9 interphase (top row), anaphase 9 (row 2), cycle 10 interphase (row 3) and cycle 10 anaphase (bottom row). F-actin is visualized with Bodipy FL phallicidin, nuclei by indirect immunofluorescence using a monoclonal anti-histone antibody, and myosin II by indirect immunofluorescence using a polyclonal antibody we prepared against the myosin tail (see Materials and Methods). The time-lapse video called mvyAnteriorBuds.mov at http://raven.zoology.washington.edu/downTheTubes/ shows the time course of periodic bud eruption and collapse.

MATERIALS AND METHODS

Embryo collection and staging

We prepared miniature egg collection plates by filling 40 mm Falcon Petri plates with 3% Bacto agar (Difco Laboratories), 20% grape juice concentrate (Welch) and 0.15% methyl paraben (Sigma) dissolved in boiling water. We placed these plates, flavored with yeast and acetic acid, as lids on empty inverted bottles containing 3- to 10-day-old adult flies (Sevelin strain). We collected eggs for 20 minutes during the daily maximum oviposition period (5-8 hours after lights-on in a 14 hours/10 hours light/dark cycle), after discarding a 45 minute pre-collection. We used Fig. 1 of Foe et al. (1993) to grossly stage eggs. We dechorionated eggs by 1.5 minute immersion in 50% bleach (Clorox), then rinsed them repeatedly in 0.8% NaCl, 0.1% Triton X-100. Since crowding dechorionated embryos results in anoxia (Foe and Alberts, 1985), embryos, aged on the collection plates, were either not dechorionated much in advance of usage or were kept well dispersed in the rinse solution. We distinguished cycle 8, 9 and 10 dechorionated embryos by the presence of pole buds, pole cells and anterior buds (Foe and Alberts, 1983) with a dissection microscope using transmitted light. We staged embryos mounted for microinjection on slides under Halocarbon oil by the position, number and size of nuclei, using a compound microscope (Foe and Alberts, 1983, 1985).

Microinjection into living embryos

Bleach-dechorionated embryos in 0.8% NaCl/0.1% Triton X-100 were transferred by pipette to parafilm (American Can Company), rinsed twice with distilled water, dried and transferred individually by forceps tip, onto fine lines of glue dried onto glass slides. The glue is double-stick Scotch tape adhesive dissolved in heptane. Rows of embryos glued to slides, after appropriate dehydration at ambient humidity, were covered with high viscosity (series 700) Halocarbon oil (Halocarbon Products Corp). Injection protocol was as described in Foe and Alberts (1983). We released embryos from the glue with several washes of n-heptane, then transferred them by pipette from heptane to fixative.

Intracellular drug concentrations cited assume a 50-fold dilution of the injected solution (Foe and Alberts, 1983) and diffusion throughout the egg. The injection buffer is phosphate-buffered saline (PBS) diluted 1/1 with distilled water. A stock cycloheximide (Sigma) solution of 10 mg/ml in water was diluted 1/10 into injection buffer. A stock cytochalasin B (Sigma) solution of 40 mg/ml in DMSO was diluted 1/100 into injection buffer. A stock colcemid solution of 4.6 mg/ml in distilled water, protected from light, was diluted 1/25 into injection buffer. Stocks were stored at –20°C.

Time-lapse recording

We used bright-field or DIC optics on Zeiss WL standard microscopes to image injected embryos under Halocarbon without coverslips with Zeiss dry Plan 16/0.35, multi-immersion, Plan NeoFluor 63/1.2 W Korr and 25/0.8 Plan Neofluor objectives. To make time-lapse movies, an Apple G3 computer using NIH-Image software recorded output of a Hammamatsu C2400 CCD camera and control box. Apple's QuickTime software (Sorensen) compressed the frames.

Embryo fixation

We use different fixation protocols to preserve different filament systems. Protocol 1, optimized to preserve myosin II and F-actin and to not deform buds, does not preserve microtubules except those stabilized by taxol or bundled into a mitotic spindle. We suspend bleach-devitellinized embryos in 4 ml of PBS and gradually add 4 ml of fix solution made of 3 parts PBS + 1 part 40% methanol-free formaldehyde (Electron Microscope Sciences Inc), while vortexing for 45 seconds, then add 4 ml heptane and agitate vigorously for 23 minutes. We stop this reaction by replacing the fix with several changes of PBS. The rational for exposing the embryos to fix prior to immersion in

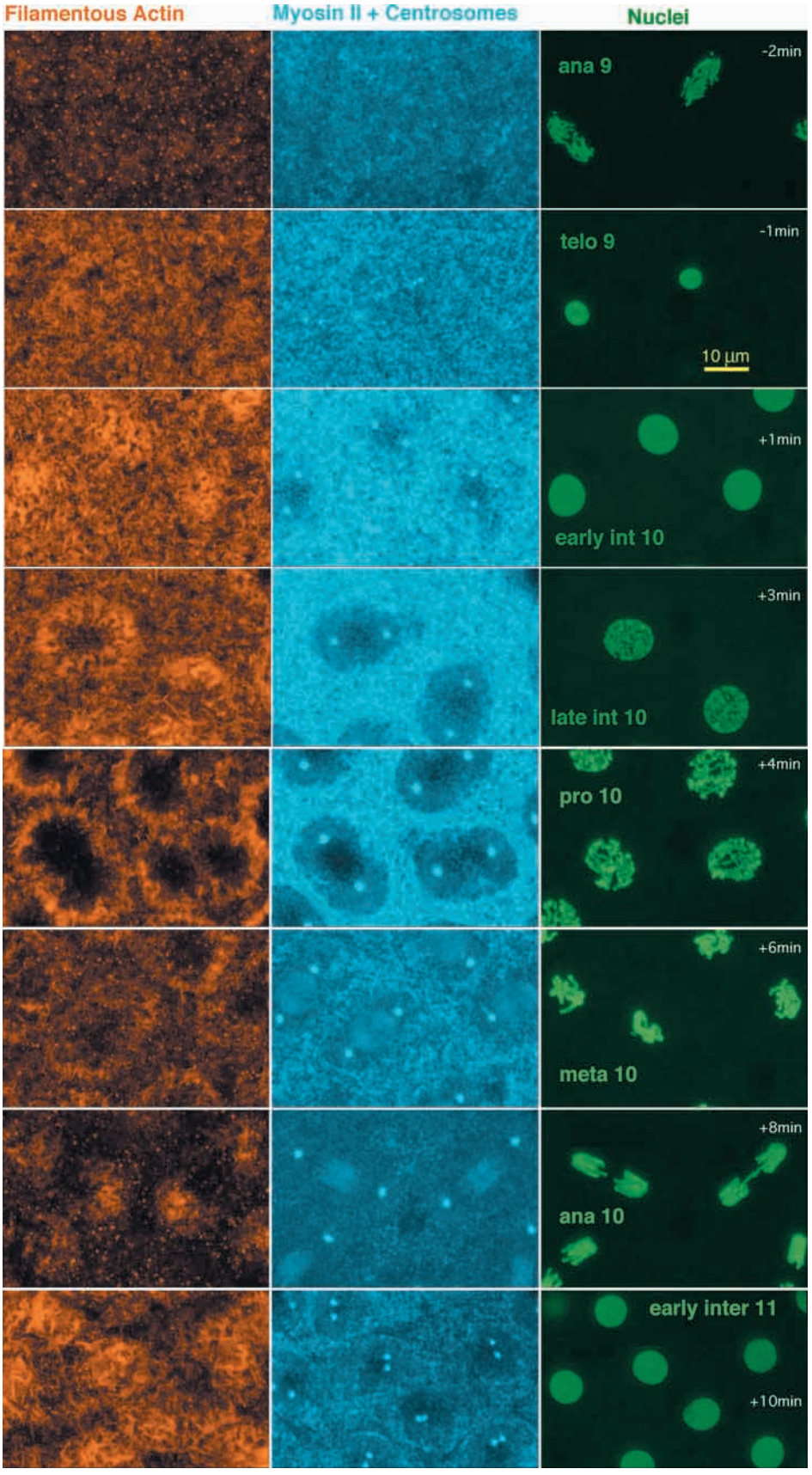

Fig. 2. F-actin (left column), myosin II and the gamma tubulin component of centrosomes (middle column) and nuclei (right column), from anaphase 9 to early interphase 11 at the cortex of a *Drosophila* embryo (colour coding as in Fig. 1). Mitotic phase, nuclear cycle and approximate time since start of cycle 10 are recorded at the right. Staining is as for Fig. 1, but with centrosomes stained with anti-gamma tubulin (generously provided by Michelle Moritz) sharing the myosin channel (central panels). The anti-gamma tubulin stains centrosomes throughout the mitotic cycle, but from metaphase through telophase, also stains the central spindle (Lajoie-Mazenc et al., 1994). Anti-myosin II alone stains spindle microtubules during metaphase and anaphase also (data not shown). To achieve quantitatively significant data, the entire sequence was collected during a single session, without changing microscope settings, from specimens that were collected, fixed, stained, cleared and mounted en masse. No images had intensity-changing filters applied to them during or after data collection except for Kalman averaging to reduce noise. As no single focal plane would show actin, myosin and nuclei, each plate is a superposition of 20 serial sections spaced 0.5 µm apart. Each stack's top is at the embryo surface except for stacks showing nuclei in the cycle 9 panels (these stacks start 13 µm below the surface to reveal nuclei still migrating). We wrote the software to make the projections.

the permeabilization solvent heptane is to permit fixative, entering through the micropyle, to fix protruding buds at the embryo anterior. Anterior buds collapse when embryos are exposed to heptane before being fixed. The low concentration of formaldehyde (5%) and absence of methanol (a component of formalin) in the fix are important to retain myosin II stainability. We manually devitellinize fixed embryos individually with tungsten needles rather than devitellinizing en masse via methanol immersion because methanol immersion ruins phalloidin stainability of F-actin.

Protocol 2, used for Figs 4, 5, 8, 9 and early interphase panels of Fig. 3, preserves microtubules, F-actin, gamma tubulin staining (centrosomes) and nuclei. Embryos are treated as above, except that protocol 2 fix is 1 part PBS + 1 part formalin (37% formaldehyde with 13% methanol). We add heptane simultaneously with fixative and fix for 13 minutes. Gross actin staining is identical in protocols 1 and 2, but detailed F-actin structure is better preserved by protocol 1. Rapid influx of heptane through the micropyle partially collapses anterior buds before fixation stabilizes them. We will publish the 3-D rendering techniques that we devised for 3-D reconstruction elsewhere.

Taxol treatment

We added taxol (Molecular Probes) from a stock solution of 2.5 mM in DMSO to embryos in 5 ml PBS to a final concentration of 10 μM. Embryos were overlaid with an equal volume of heptane (to permeabilize vitelline membrane) and shaken for 90 seconds. Fixation by protocol 1 (for Figs 6, 7) or protocol 2 (for Fig. 8) was commenced 90 seconds after taxol application. Permeabilization is not instantaneous so we estimate that the live embryo exposure to taxol is between 1 and 1.5 minutes.

Myosin II isolation

Extract of 0- to 4-hour-old *Drosophila* embryos was passed over filamentous actin or albumin control columns. Column preparation, embryo extracts and chromatography conditions were as described previously (Miller et al., 1989, 1991). Proteins, eluted with 1 M KCl, 1 mM ATP, 1 mM $MgCl_2$, were further separated by SDS-PAGE using preparative gradient gels. Individual bands were excised and used as antigens for antibody generation in mice. Myosin II migrated at approximately 200 kDa.

Cloning of *Drosophila melanogaster* myosin II

Mouse antibody #4 from Miller et al. (1989) was used to screen a λZap expression library constructed from *Drosophila* ovary poly(A)$^+$ RNA (Hay et al., 1988). The library was screened using minor modifications of procedures described by Huynh et al. (1985). Clones from the screen were sequenced using fluorescently labeled chain terminator nucleotides with an Applied Biosystems 373 automated sequencer. The screen produced two unrelated cDNA clones, one of which is approximately 1.3 kb in length and encodes amino acids 959-1496 of the non-muscle myosin heavy chain tail (Ketchum et al., 1990; Kiehart and Feghali, 1986).

Myosin II antibody generation

A glutathione S-transferase (GST) fusion with the myosin II tail fragment was generated using a pGEX expression vector (Smith and Johnson, 1988). We used this fusion protein to generate polyclonal antibodies in rabbits. Antibodies were affinity purified by passage over columns of immobilized fusion proteins. The serum was first depleted of anti-GST antibodies by repeated passage over a column of GST protein and then passed over a column containing the myosin fragment, as detailed in Field and Alberts (1995).

Staining and confocal microscope imaging

Micrographs in Figs 1 and 2 were made on a BioRad Radiance Plus laser scanning confocal microscope (LSCM), with three photodetectors. All others were made on a two-photodetector BioRad MRC-600 LSCM, and were all made using a Nikon plan apochromatic 60/1.4 oil immersion objective. Our nuclear staining protocol enables the BioRad MRC-600 to distinguish chromatin staining from other red and green channel probes, thus differentiating three probes using just two photodetectors.

We block fixed embryos for 30 minutes with normal goat serum (50 μl/ml in PBT; PBT is PBS with 0.1% Triton X-100), react with 1/750 polyclonal rabbit anti-myosin and 1/1500 anti-gamma tubulin (to visualize centrosomes) for 4-6 hours at room temperature, wash with PBT for 3× 5 minutes plus 3× 30 minutes, then stain the rabbit antibodies with 1/750 Alexa 568-conjugated goat anti-rabbit IgG (Molecular Probes Inc) or, for three-photodetector imaging, with 1/750 Cy5 goat anti-rabbit (Jackson Immuno Research Labs). We incubate embryos already stained with antibodies in DNAase-free RNAase at 1 mg/ml for 1.5 hours at 37°C, then rinse 3× in PBT and add between 1.0 and 3.0 μl/ml of a 15 mg/ml stock solution of propidium iodide in DMSO to the phalloidin reaction solution (see below) and incubate at room temperature for 1-3 hours. The goal is to obtain a sufficiently low level of chromatin staining by propidium iodide to be *undetectable* by the LSCM when excited by 1% of the laser intensity, yet staining sufficient to be seen at 10% excitation after the other probes have been bleached away (see details in section on confocal microscopy below). For imaging with three photodetectors (Fig. 2), nuclei are stained with mouse monoclonal anti-histone (Chemicon) at 1/1500 and visualized with 1/1000 rhodamine Red-X goat anti-mouse (Molecular Probes).

We stain F-actin with BODIPY-Fl phallicidin (Molecular Probes), 300 units of which dissolved in 1.5 ml methanol and stored at –20°C constitute our stock solution. Five 10 μl aliquots of this stock are vacuum dried at room temperature, redissolved in PBT, pooled to give 1 ml of solution and embryos already stained with antibodies are suspended in this solution. If nuclei are to be visualized, these embryos were previously treated with RNAase and propidium iodine is added to the phallicidin solution. Embryos were incubated in the phallicidin/propidium iodide solution for 1 to 3 hours at room temperature and then rinsed for 1 hour in PBT. Variation in the staining duration does not affect staining. Prolonged rinsing washes out propidium iodide and diminishes the phallicidin staining, especially that of delicate cortical actin fibers (because phallotoxins can exchange off of F-actin). Therefore phallotoxin or propidium-stained embryos were cleared and mounted immediately after rinsing or, if stored, were kept in small volumes of PBS.

To visualize deep internal cytoskeletal structures, we clear and mount embryos in Murray's mounting medium (2 parts benzyl benzoate: 1 part benzyl alcohol). This matches the refractive index of *Drosophila* yolk. Unless all salt is removed before transferring embryos into Murray's medium, propidium iodide-stained nuclei will not fluoresce. We transfer embryos from PBT to 1/40 PBS in three dilution steps each of 5 minute duration. Because methanol and ethanol damage the phallicidin-stainability of F-actin, we dehydrate embryos in isopropanol, with a minimum exposure. While gently vortexing, we pipette 0.3 ml of 100% isopropanol into an Eppendorf tube containing the embryos in 0.15 ml of 1/40 PBS. After allowing the embryos to settle for 1.5 minutes, we pipette them onto a polylysine-coated slide, and then transfer the slide through a dehydration series of 85%, 95% and 2× 100% isopropanol (allowing 20-30 seconds per step), and then through three 5 minute changes of Murray's medium. The preparation is covered with a number 1.5 cover glass and sealed with 5 minute Epoxy glue (Devcon) to give a semipermanent preparation. Epoxy adheres to glass slides sufficiently to make a seal only after removing excess Murray's medium (with xylene-soaked swabs).

We coat slides with polylysine by dipping them in a solution of 100 ml water, 60 mg poly-L-lysine hydrobromide (Sigma), 200 μl Photoflo (Kodak). Dipped slides are air-dried, rinsed in distilled water and redried. We make slides fresh every two weeks because poly-lysine slides slowly lose their adhesivity. Shims, made from Scotch

Brand 425 aluminum tape, placed beside embryos support cover glasses to prevent embryo deformation.

Confocal microscopy

How do we differentiate nuclear staining from the staining in the red (myosin) and green (actin) channels using only the MRC 600's two photodetectors? The F-actin and myosin II images are obtained by exciting with 1% of the laser intensity at the 488 nm and 568 nm laser lines, respectively, and collecting, into the two photodetectors, light emitted at 522 nm and 585 nm, respectively. Then we bleach away the F-actin and myosin II probes by exciting the sample with all laser lines at 10% laser strength. The dim, but more photostable, propidium iodide probe survives this. We imaged it at 10% laser intensity by exciting at 488 nm and collecting the emission light at 585 nm. Images were collected using a dual channel (K1/K2) filter block but excited with one laser line at a time to minimize bleed-through. Nuclei in Figs 1, 3, 4, 5 and 6 were all imaged in this way. The micrographs in Figs 1 and 2 were obtained with a BioRad Radiance Plus confocal microscope, which allows viewing triple probes in the usual way. Where indicated in the captions, images represent stacks of successive optical sections.

RESULTS

Mitotic cycle progression and centrosome-nucleated microtubule arrays correlate with spatial reorganizations of cortical F-actin and myosin II in the *Drosophila* syncytial blastoderm

Fig. 1 comprises laser scanning confocal microscope (hereafter LSCM) sectional views of anterior ends of *Drosophila* embryos showing anaphase and interphase of cycle 9 (before centrosomes, microtubules and nuclei reach the cortex) and cycle 10 (the first round of bud formation and breakdown). In cycle 9, myosin II staining concentrates in a cortical rim during interphase but leaves the cortex during anaphase (myosin, row 1 versus row 2). Likewise, F-actin concentrates during interphase 9 in a cortical rim, which attenuates greatly during anaphase 9. Throughout interphase 9, with no nuclei/asters near the cortex, cortical myosin II and F-actin co-localize. We observed similar waxing and waning of cortical F-actin and myosin II, co-localized, synchronized with globally synchronous mitotic cycles, in cycle 8 (not shown). Migrating nuclei with microtubule arrays reach the cortex 1 minute after interphase 10 begins (Foe and Alberts, 1983). As telophase 9 ends and interphase 10 begins, F-actin and myosin II re-accumulate co-localized to high levels in a spatially uniform cortical rim (not shown in sectional view, but see Fig. 2, row 2). 2 minutes after nuclei reach the cortex, cortical F-actin and myosin II are no longer co-localized but occur in the *complementary* patterns shown in Fig. 1, row 3. Myosin II occurs at high levels between buds, but vacates the cortex where buds now protrude (row 3), while F-actin attains high levels precisely on the domes of the buds that myosin II vacated. During anaphase 10, cortical levels of F-actin and myosin II are globally low. Cortical F-actin re-accumulation begins first near centrosomes at anaphase/telophase (Fig. 1, row 4). Regardless of cortical fluctuations, high levels of myosin II staining occur throughout the embryo interior (Fig. 1, rows 1-4); myosin-dark holes are where yolk particles exclude the myosin probe. When myosin dissociates from the cortex, it transiently boosts the concentration of myosin immediately beneath the cortex, but does not significantly boost the concentration of internal myosin globally, presumably because it is dispersing into an ocean of cytoplasmic myosin filling this large cell. Throughout the interior cytoplasm, F-actin occurs diffusely, and additionally in particles, but at lower levels than cortically. von Dassow and Schubiger (1994) have described in detail the cyclic reorganizations of internal F-actin during nuclear migration.

Fig. 2 comprises surface views of *Drosophila* embryos at about 50% egg length, as overlays of multiple LSCM single sections, showing in finer temporal resolution the rapidly

Fig. 3. Reconstructions of 42 μm wide by 28 μm high by 22 μm deep volumes of *Drosophila* syncytial blastoderm during early (rows 1-3) and mid (rows 4-6) interphase of cycle 10. Figs 3-5 facilitate fusing the stereopairs by either crossing or diverging your eyes. The left eye's view is in the center column, flanked on both sides by the right eye's view. Cover the right column to fuse the left and center images by crossing your eyes. Cover the left column to fuse the center and right images by diverging your eyes. Alternatively, interactive virtual objects available at http://raven.zoology.washington.edu/downTheTubes/ provide incomparably better versions of Figs 3-5, which bypass any need to fuse stereopairs. Microtubules are yellow, F-actin red, myosin II blue, nuclei green, centrosomes magenta or white, and yolk particles gray. The upper two rows show apical views at early interphase 10 without and with the cortical layer of F-actin rendered. Row 3 is a basal view of the same reconstruction. While most microtubules appear to run back towards centrosomes, very few actually connect to them. Spindle remnants persist into early interphase. Rows 4-6 show three views all from the same apical vantage at mid-interphase. Row 4 shows myosin II, centrosomes, nuclei and yolk particles. Row 5 shows F-actin instead of myosin II. Row 6 shows myosin II and F-actin superimposed. These 3-D reconstructions result from extensive image processing of three merged stacks of raw data, each with hundreds of laser scanning confocal micrographs spaced 0.2 μm apart. Computer software that we wrote, to be described elsewhere, segments micrographs, picking out structures of interest and rendering as transparent low-level fluorescence and non-specific background staining to facilitate seeing deep into the volume reconstructed. In particular, we have rendered invisible a general low level of F-actin and of myosin II staining throughout all the cytoplasm and the viewer must imagine this permeating the much brighter regions of F-actin and myosin II probe shown. With one exception, every part of each the 3-D reconstruction is actual data the LSCM recorded (not a mathematized representation of the data). The exception is that the centrosomes are mathematical spheres placed where gamma tubulin staining shows the centrosomes to be (actual gamma tubulin staining is shown in the middle column of Fig. 2.) Fig. 2 shows surface views at the same stages of mitotic cycle 10. We adjusted the brightness of the actin in Figs 3-5 to maximize visibility of F-actin structures, instead of accurately portraying differences in relative probe brightness between mitotic cycle phases as in Fig. 2. When locating microtubules and parts of microtubules in these reconstructions, our software found many thousands of short (< 1/2 μm) segments of microtubule probe scattered everywhere throughout the cytoplasm (but most concentrated near the cortex). These bits of microtubule 'chaff' were not arranged along any detectable curve that might have constituted a previously long microtubule clipped into fragments. However, we do not believe this is non-specific anti-tubulin staining because microtubule chaff is affected by drugs that affect microtubule polymerization dynamics. We suspect this microtubule chaff results from microtubule nucleating events that fail to produce long microtubules when microtubule minus ends are not stabilized. Rendering the microtubule chaff in the reconstructions makes a blizzard of tiny particles, lacking detectable coherence, which obscures vision deep into the reconstruction. We therefore erased it in the reconstructions.

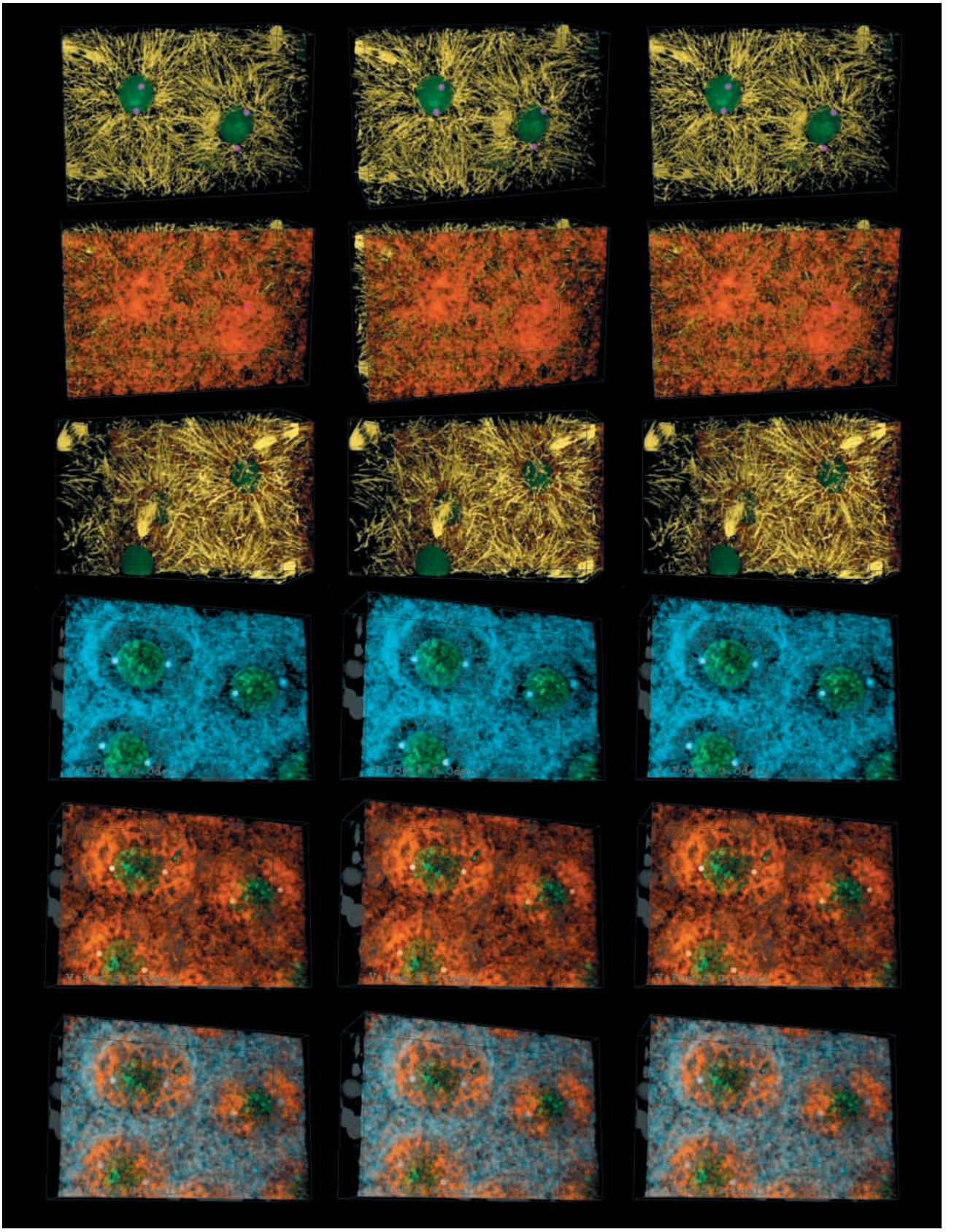

Fig. 3. For legend see p. 1771.

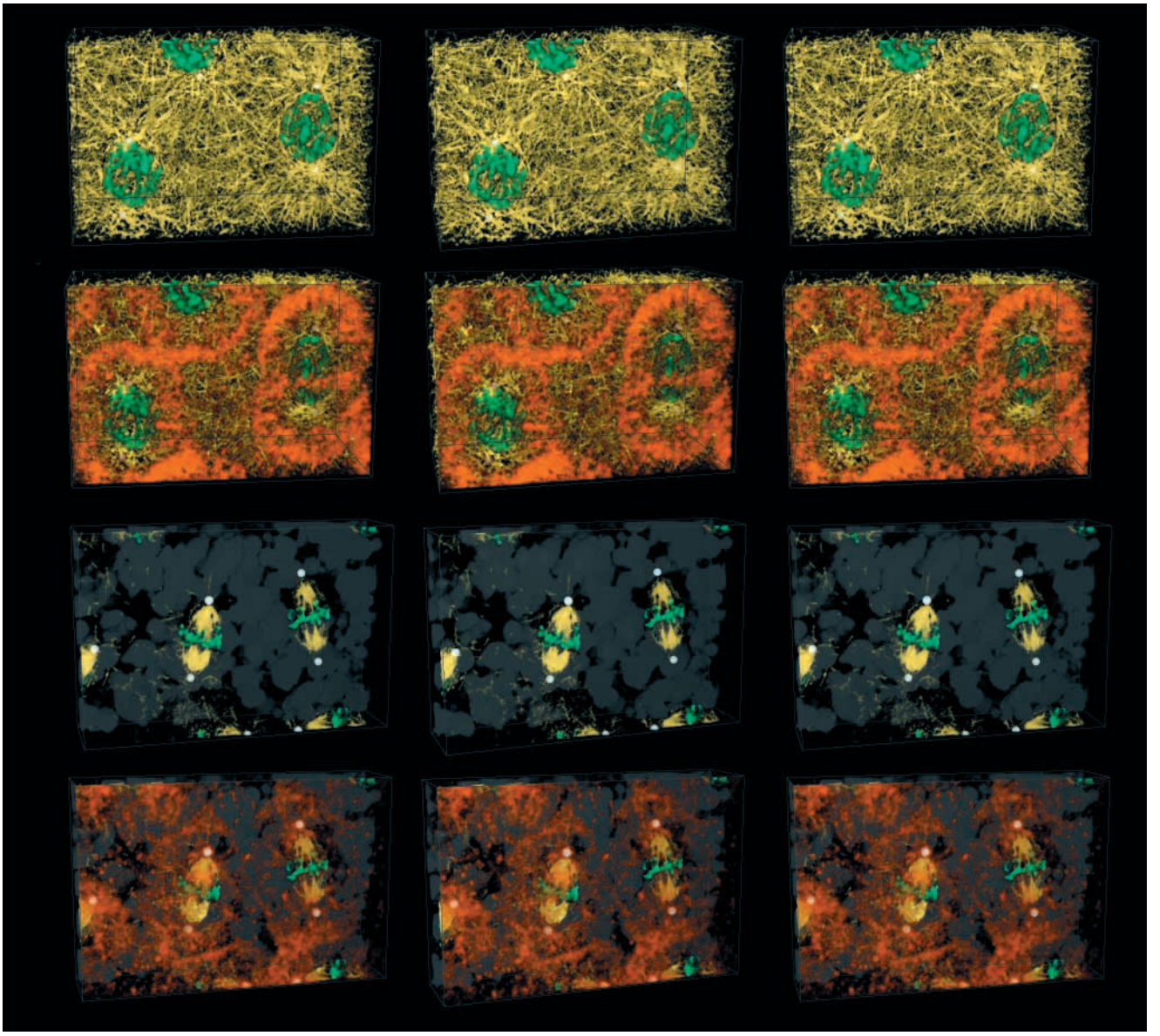

Fig. 4. 3-D reconstructions (color code and general features as in Fig. 3.) of prophase 10 (rows 1 and 2) and metaphase 10 (rows 3 and 4), both from apical vantages. The prophase density of microtubules is higher than at any other phase, but few microtubules connect back to centrosomes. Microtubule geometry is extremely complex in prophase compared to early interphase 3 minutes earlier (in Fig. 3), and compared to metaphase 2 minutes later, when microtubules are scarce, except for spindle microtubules. In prophase, F-actin forms figures of eight linked rings above some nuclei, and ellipsoidal rings above others, always with the centrosomes at the foci.

changing organizations of F-actin, myosin II, centrosomes and chromatin just prior to and during the first cycle of bud formation. Relative intensities of the myosin II and F-actin probes in Figs 1 and 2 are quantitatively accurate representations of the intensity changes as the mitotic cycles progress. When migrating nuclei with associated microtubule arrays first reach the periphery early in interphase 10, myosin II staining disappears from a small region immediately above the nuclei (row 3) and, during the next 3 minutes of interphase and prophase, the holes vacated by myosin II staining enlarge into oblong holes (rows 4 and 5). During metaphase and anaphase, the cortical myosin staining dims (rows 6-7), then, during telophase (row 8), myosin staining returns brightly to the cortex except near centrosomes where it remains dim. We interpret holes in the cortical myosin pattern, appearing in the cortex precisely when/where microtubule arrays first contact the cortex, as implying an interaction between myosin II and microtubules. Lajoie-Mazenc and colleagues showed anti-gamma tubulin concentrates on the spindle during metaphase and on the midbody remnant from anaphase through telophase (Lajoie-Mazenc et al., 1994). Therefore, the staining of the spindles in Fig. 2 in the middle columns of metaphase 10 and anaphase 10 may be partly due to anti-gamma tubulin labeling, but only partly, because we find that embryos stained with anti-myosin II in the absence of anti-gamma tubulin also show the spindle and midbody staining pattern displayed in rows 6-7 of Fig. 2. Single section images (not shown) reveal that the cytoplasmic myosin staining at anaphase 10 and early

telophase (shown as multisection projections in Fig. 2), in addition to the midbody and cortical staining, includes a low level but discernable accumulation of myosin staining on the forming aster. We obtain the same staining patterns with our polyclonal antibody prepared against a part of the *Drosophila* myosin II tail and with a polyclonal anti-myosin prepared against whole myosin heavy chain (the generous gift of Daniel Kiehart; data not shown).

As migrating nuclei, centrosomes and microtubule arrays approach the cortex, they affect cortical F-actin differently than myosin II. F-actin accumulates between centrosomes and the plasma membrane, forming 'caps' in the regions that myosin II staining vacates (Fig. 2, row 3, compare left red panel – F-actin, with center blue panel – myosin II; also row 3 of Fig. 1). During the next 3 minutes these small caps of actin enlarge in outer diameter and hollow out centrally above each centrosome (rows 3-5 of Fig. 2; also see rows 2 and 5 of Fig. 3 and row 2 of Fig. 4). During metaphase, the cortical F-actin staining attenuates globally with the ghosts of the prophase F-actin rings persisting longest (row 6 of Fig. 2; also row 4 of Fig. 4). Actin staining remains dim globally during anaphase with re-accumulation beginning in the cortex overlying centrosomes before it does so elsewhere (row 7 of Fig. 2; row 4 of Fig. 1; also rows 2 and 4 of Fig. 5). F-actin accumulation into caps accelerates during telophase 10 and early interphase 11 (row 8 of Fig. 2). (For earlier descriptions of F-actin kinematics see Karr and Alberts, 1986; Kellogg et al., 1988; Warn et al., 1984.)

In Fig. 2, juxtaposing eight sequential phases of the mitotic cycle clearly exhibits the global waxing and waning of cortical F-actin and myosin II. These changes are spatially homogeneous in cycle 9. During cycle 10, cortical concentrations of myosin II between buds resembles the *same-phase,* cycle 9, concentrations seen uniformly across the cortex. Both F-actin and myosin II staining attenuate during metaphase, reach a minimum during anaphase, rapidly rebuild during telophase, and maintain a high level during interphase and prophase (see also Fig. 1). These wild-type kinematics suggest the mitotic oscillator modulates F-actin and myosin II polymerization dynamics, and/or the attachment of these molecules to the cell cortex, enabling potentially higher levels of actomyosin contractility from telophase through interphase, and suppressing it during metaphase and anaphase.

Figs 3, 4 and 5 comprise a sequence of stereopair 3-D reconstructions that we made of small volumes of the syncytial blastoderm in fixed and staged embryos. These show how the arrangement of microtubules changes through the mitotic cycle, and how the microtubule kinematics correlate with the spatial rearrangements of F-actin and myosin II in cycle 10 described above. The relative intensities of the myosin II and F-actin in these 3-D reconstructions are not accurate because LSCM gain was set to reveal topological detail in each reconstruction rather than to show intensity changes from one phase of the cycle to the next. Figs 3-5 show microtubules running in all directions. No single focal plane of a 2-D micrograph can portray accurately their 3-D geometry. The conclusions that we glean from Figs 3-5 are found throughout the text, especially in the Discussion section. QuickTime movies and interactive virtual reality objects, from which Figs 3-5 show selected frames, are available at and http://raven.zoology.washington.edu/downTheTubes/. These 100-200 megabyte files merit downloading because the interactive full-rotation vision of the blastoderm cytoskeleton's geometric complexity that they communicate far surpasses the glimpses that Figs 3-5 provide.

The 3-D reconstructions in Figs 3-5 and the surface views in Fig. 2 are at about 50% egg length. Only at the anterior and posterior poles of the embryo does sufficient space exist between the plasma membrane and the egg shell for buds to protrude into (as in Fig. 1). The flatness of the egg surface in Figs 2-5 is caused by the plasma membrane pressing against the nearly non-deformable vitelline membrane, whose curvature is so slight as to be nearly imperceptible across the 42 μm width of the region imaged. Except at the poles, invaginations of the plasma membrane are possible but protrusions are not. Our 3-D reconstructions of cycle 12 and 13 embryos (not shown here, but see http://raven.zoology.washington.edu/downTheTubes/ for a 3-D reconstruction of metaphase 12) confirm the common understanding that deep invaginations of the cortex, pseudocleavage furrows, form between adjacent nuclei during later syncytial cycles as nuclei become closely packed. Pseudocleavage furrow invaginations along the sides of the embryo are *mechanically* equivalent to buds protruding out above the egg surface as occurs at the anterior pole of the embryo starting in cycle 10 (Fig. 1). In this paper, we confined our investigation of cytoskeletal kinematics to cycles 10 and earlier precisely because the cortex (except at the poles) remains nearly planar during those cycles. Therefore deformation of the cortex cannot play any important role in *causing* the dramatic spatial reorganization of myosin II and F-actin shown in Figs 2-5. Rather the spatial rearrangements of myosin II, F-actin and other cytoskeletal proteins into the kind of patterns shown in Figs 2-5 almost certainly cause invagination of pseudocleavage furrows in later cycles (see Discussion).

The F-actin and myosin II reorganizations of Fig. 2, rows 3-5, and Figs 3 and 4, take only 3 minutes, reminiscent of the time it takes a mitotic apparatus to induce a cleavage furrow (reviewed in Rappaport, 1996). Another interesting feature of the cytoskeletal kinematics described above is that they appear always to act to attenuate the potential actomyosin-based contractile strength of the cortex. During interphase, when global amounts of cortical F-actin and myosin II are greatest, the highest concentrations of these two key parts of the actomyosin contractile machinery are kept mostly separate. During metaphase, the F-actin and myosin II that remain at the cortex disperse toward spatially uniform co-localization but, at this phase of the mitotic cycle, cortical concentrations of F-actin and myosin II plummet, attenuating actomyosin contractile potential by different means. In telophase, when myosin II reconcentrates at the cortex, it vacates the regions overlying the centrosomes where F-actin is strongly re-accumulating. Myosin II and F-actin always colocalize at the cortex and throughout the embryo's cytoplasm. Due to their global disappearance during mitosis and their spatial reorganization into near complementary patterns at other phases, however, the level of myosin II and F-actin colocalization remains always low relative to what it could be. When buds form (telophase through prophase), the cortex between buds (which in later cycles will invaginate as pseudocleavage furrows) are the zones where myosin II and F-actin do co-localize, though F-actin concentrations

elsewhere are higher; this point is especially apparent in sectional views (Fig. 1, row 3).

Microtubule asters with no centrosomes cause reorganization of nearby cortical F-actin and myosin

Meiotic sisters of the female pronucleus, the polar body nuclei, persist until cycle 10 near the dorsal cortex of *Drosophila* embryos. These lack centrosomes and arrest in permanent metaphase-like configurations without nuclear envelopes, apparently after completing S-phase of their first mitotic cycle (see Foe et al., 1993). The condensed chromosomes from one, two or all three polar bodies form large starbursts with chromosomes joined near their kinetochores (Fig. 6C,E). In wild-type embryos, sparse arrays of short microtubules form around these polar bodies, organized presumably by chromosomes, as no centrosomes are present. The polarity of microtubules in these arrays has not been established. However, chromatids segregate normally during anaphase on centrosome-less spindles (Bonaccorsi et al., 1998; Matthies et al., 1996; Megraw et al., 1999), so it is likely that microtubules nucleated from chromosomes are oriented normally, i.e. with plus ends at kinetochores. If so, microtubule arrays nucleated from polar body chromosomes would form 'asters' with polarity opposite that of a centrosome-nucleated asters. In the reversed aster, the minus ends of microtubules would form the outer perimeter of the aster while the plus ends cluster at the aster's center, near kinetochores, as cartooned in Fig. 11B.

By observing the effect this peculiar aster has on nearby F-actin and myosin, we proposed to answer two questions. (1) Can microtubule asters with no centrosome nucleating them influence spatial reorganization of nearby F-actin and myosin? The answer is, yes. When polar bodies lie close to the cortex, the immediately adjacent cortex is often depleted of both F-actin and myosin. Fig. 6D shows a surface view of myosin II depletion above the polar body of an embryo fixed in late interphase of cycle 8. Myosin depletion above sparse polar body microtubule arrays tends to be less pronounced than myosin-depletion over the denser microtubule arrays nucleated from centrosomes. Taxol treatment, by blocking microtubule disassembly, inhibits microtubule dynamic instability, promotes microtubule growth and induces non-centrosomal microtubule nucleation (Horwitz et al., 1986). Fig. 6A shows, in sectional view, F-actin depletion from the cortex above the polar body in an interphase 8 embryo briefly treated with taxol (see Materials and Methods). Though taxol rapidly increases the number of microtubules associated with polar body nuclei (Fig. 6B), cortical F-actin depletion above polar bodies in embryos fixed without prior taxol treatment (not shown) and after a 1-1.5 minute exposure to taxol are similar. The *depletion* of cortical F-actin above polar body microtubule arrays contrasts with F-actin *accumulation* into caps or rings near centrosome-nucleated microtubule arrays of zygotic nuclei.

(2) Do microtubule asters clear F-actin from their centers, concentrating it at their perimeter (as do normal cycle 10 asters shown in Figs 3-5), regardless of the polarity of the microtubules in the aster? To answer this question, we increased the number of microtubules in the polar body asters by brief taxol treatment (Fig. 6B). Notwithstanding the very high density of microtubules in the taxol-stabilized polar body aster, this aster concentrates F-actin at its center (Fig. 6A) rather than re-locating cortical actin towards the perimeter (as in Fig. 2 rows 3- 5). Indeed, even without taxol, low concentrations of F-actin are discernable at the internal core of the normal sparse polar body asters by the end of interphase (not shown). We thus tentatively conclude that it is the polarity of the microtubules in an aster that determines where F-actin concentrations re-locate to. To explain the effect microtubule arrays have upon F-actin reorganization in all of Figs 1-6, it appears that F-actin, or a signal to polymerize it, moves toward the plus ends of microtubules in oriented arrays.

Drug-induced amplification/creation of cortical microtubules has profound and rapid effects on cortical F-actin

We find that treating pre-cycle10 embryos with taxol for 1-1.5 minutes causes a dense disorganized mat of short (2-10 μm) microtubules to form *everywhere* within about 2 μm of the cell cortex regardless of mitotic phase (shown in sectional view in Fig. 6B and in surface view in Fig. 8A), and causes diminution of centrosome-nucleated microtubules deep inside embryos (presumably by polymerizing at the cortex, where taxol first impinges tubulin dimers that would otherwise make interior microtubules). Earlier studies (Karr and Alberts, 1986) construed this to be the normal microtubule organization in preblastoderm embryos, but our improved fixation techniques show that this mat of cortical microtubules is an artifact of exposing the permeabilized embryo to taxol. Taxol treatment before cycle 10 lets us assay how the rapid genesis of myriad randomly oriented microtubules affects F-actin. Fig. 7 shows single-section high-magnification LSCM micrographs of phalloidin-stained embryos taken in the plane of the embryo surface, with untreated embryos (left) and embryos after a 1-1.5 minute exposure to taxol (right). Taxol administered during interphase 9 induces redistribution of cortical F-actin into long fibers (Fig. 7A,B) over the entire embryo surface (except above polar bodies where cortical F-actin is depleted). Taxol treatment during anaphase 9, (when cortical F-actin levels drop; Fig. 7A-C), induces dramatically fewer and thinner cortical actin fibers than does treatment during interphase (Fig. 7B versus D).

Taxol immersion during cycle 10 (with nuclei and associated microtubule arrays at the cortex) causes redistribution from fewer long, to more numerous but shorter, microtubules in centrosome-nucleated cortical microtubule arrays. It also induces randomly oriented short microtubules in the cortex between buds. Taxol immersion during cycle 10 interphase induces actin fibers over the entire surface but most densely at the actin caps that normally form above centrosomes (Fig. 7E,F). During prophase, taxol induces cortical actin fibers from the F-actin rings that encircle buds and in the cortex between buds, but very few in actin-depleted bud crowns (Fig. 7G,H). Taxol treatment during anaphase 10 resembles anaphase 9 in inducing few if any cortical actin fibers (anaphase 10 not shown). Taxol treatment at telophase 10 induces many F-actin fibers to grow from the forming actin caps, while few grow in the actin-poor zones between caps (Fig. 7J). In summary, in response to taxol stabilization of microtubules, F-actin fibers form wherever the cortical F-actin concentration is high; in cortical regions normally depleted of F-actin because of

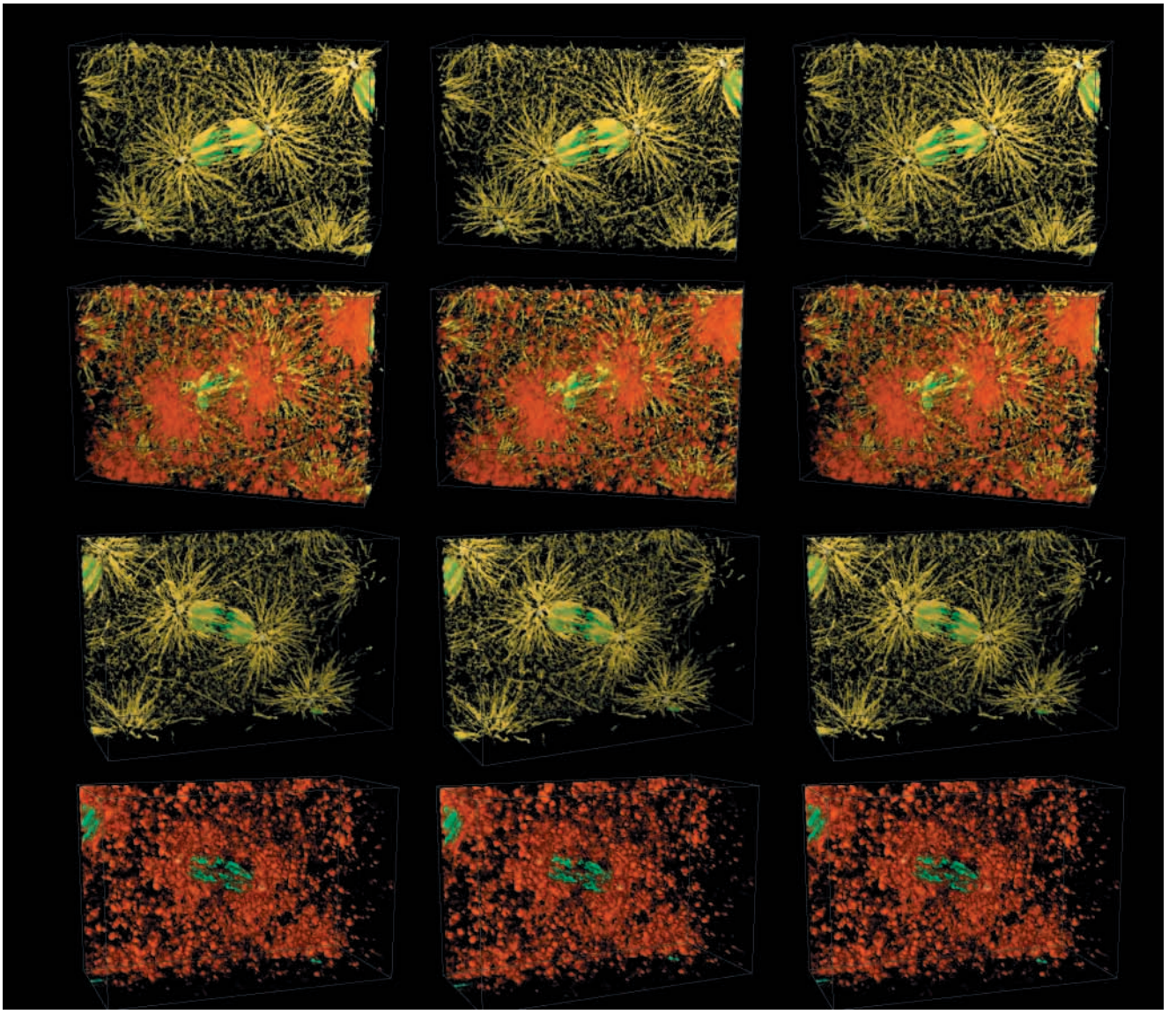

Fig. 5. Apical views (top two rows) and basal views (bottom two rows) of a 3-D reconstruction at anaphase 10 (color code and general features as in Fig. 3). We substantially boosted F-actin's brightness to make its spatial organization visible. (Fig. 2 shows correct relative concentrations of F-actin and myosin in different mitotic cycle phases.) Most microtubules trace back to the centrosomes that nucleated them. The centrosomes, already replicated, are close together at the spindle poles. F-actin caps are visible in row 2 as they begin to form directly over centrosomes. In row 4, with microtubules invisible, the elevated concentration of F-actin in the regions occupied by asters is easy to see. F-actin particles are distributed throughout the cytoplasm, far from the cortex, but are most concentrated amongst the forming astral microtubules.

microtubule or mitotic phase effects, taxol does not promote actin fiber formation. The effect de novo polymerization of microtubules has upon cortical F-actin organization, and the rapidity of that effect, implies an interaction between these two principal filament systems.

We detect no obvious co-alignment between the actin fibers and the short microtubules that taxol induces in the cortex of pre-cycle 10 embryos (Fig. 8A-C). Once nuclei and microtubule arrays approach the cortex, taxol amplifies existing microtubule arrays, presumably by reducing microtubule depolymerization. In the presence of these dense stable arrays, the usual interphase 10 actin disks and rings often have 'tufts' extending from their outer edges (Fig. 8E). Some of these tufts overlie microtubules (see Fig. 8D-F), as would be expected if F-actin were being pulled out along microtubule tracks. Elsewhere, however, actin fibers exist separate from underlying microtubules. Further study on F-actin/microtubule spatial relationships should be done in live embryos where the dynamic natures of actin fibers and microtubules do not complicate interpretation. Just permeabilizing membranes with heptane – essential for our taxol treatment – has little effect on F-actin organization, but it abolishes most of the cortical myosin II staining. This precluded determining what effect taxol-induced ectopic microtubules have on myosin distributions with our experiment.

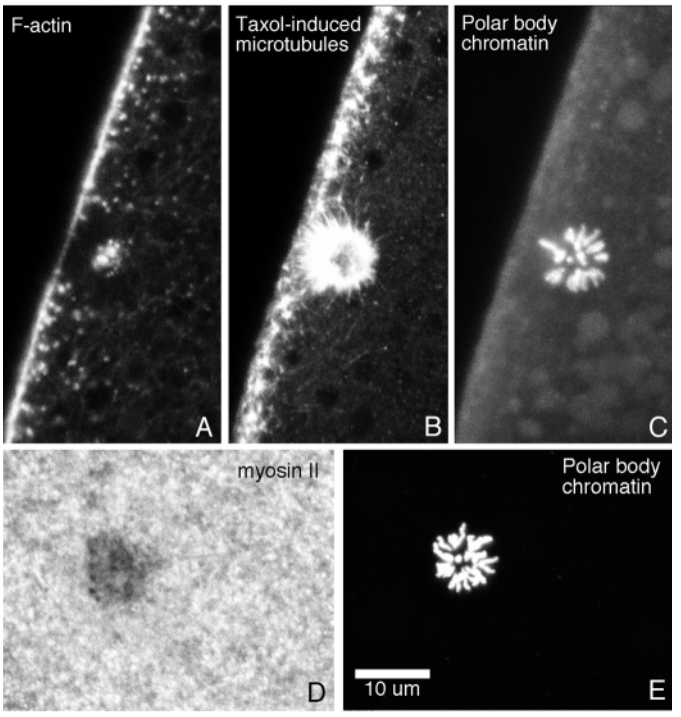

Fig. 6. LSCM micrographs showing polar body nuclei and associated cytoskeletal elements. (A-C) Mid-sagittal sections (dorsal to the left) of the same cycle 8, taxol-treated embryo. No zygotic nuclei have reached the cortex, so there are no centrosomes near the structures shown here. Taxol induces the formation of short microtubules at the cortex and enhances the microtubule array associated with polar body chromosomes (B). Where the dense array of induced microtubules contacts the cortex, that region is depleted of F-actin, as is the entire spherical region occupied by the aster, except that F-actin is concentrated in the center of the microtubule aster. (C) The chromatin panel is a superposition of 22 confocal micrographs spaced 0.5 μm apart (spanning the approx. 11 μm diameter polar body cluster). The F-actin (A) and microtubule (B) panels are each superposition of 3 such sections centered around the polar body center. (D) A single optical section surface view of the hole in cortical myosin II staining above the polar body nucleus of another late interphase 8 embryo whose polar bodies (E) are shown as a projection of 22 confocal micrographs spaced 0.5 μm apart. The embryo shown in D,E was fixed and stained without taxol treatment.

Prolonging interphase cytoskeletal dynamics removes F-actin from the cortex when microtubules are present, and also implicates F-actin in binding microtubule arrays and nuclei to the cortex

Early mitotic cycles proceed so rapidly in *Drosophila* that cytoskeletal geometry is always changing rapidly. No phase lasts long enough for us to glimpse what equilibrium the cytoskeleton might approach during a long-lasting phase. In syncytial *Drosophila* embryos, protein synthesis inhibitors cause interphase arrest, presumably by inhibiting cyclin synthesis. In early cycle 13, we microinjected cycloheximide (intracellular concentration about 20 μg/ml) to inhibit protein synthesis, thereby causing permanent arrest in interphase 13. Time-lapse videorecordings show that, beginning about 1 hour after cycloheximide injection, nuclei begin leaving the egg periphery. Fixing and staining injected embryos just as nuclei disconnect from the cortex reveals that F-actin that would normally coat the cell's cortex densely during interphase (Fig. 9A, top panel), has left the cortex (Fig. 9B, top panel) and has aggregated deep inside the embryo around the distal ends of interphase microtubules (Fig. 9B). In regions where patches of nuclei/asters fall away from the cortex, cortical F-actin reappears precisely in the locations that microtubule arrays have vacated (cf. upper and lower panels of Fig. 9B). Injecting colcemid alone into syncytial *Drosophila* embryos disrupts microtubules and arrests the mitotic cycle in metaphase with chromatin permanently condensed (Zalokar and Erk, 1976). But, simultaneous microinjection of cycloheximide (to 20 μg/ml) plus colcemid (to 100 μM) early in interphase, causes interphase arrest (the chromatin remains decondensed and the nuclei spherical) *and* microtubule depolymerization (Fig. 9C), i.e., while cycloheximide causes interphase arrest, colcemid eliminates microtubules. During this permanent interphase 13 with microtubules absent F-actin remains concentrated at the cortex even 3 hours after the injection (Fig. 9C top panel), though nuclei have become displaced from the cortex (Fig. 9C bottom panel).

Because loss of cortical F-actin brought about by injection of cycloheximide is associated with detachment of nuclei from the cortex, we tested whether loss of cortical F-actin by other means has the same effect. We microinjected cytochalasin B into cycle 8-9 *Drosophila* embryos to an intracellular concentration of 5μg/ml. By inhibiting actin polymerization (Mabuchi, 1986), cytochalasin leads eventually to F-actin depolymerization. We monitored subsequent development by time-lapse movies, then fixed the embryos in late cycle 13 and stained to reveal F-actin. Fixed preparations show that, by cycle 13, very little filamentous actin remains and nothing resembling normal actin caps or rings exist (not shown). Our time-lapse movies show that, in cytochalasin-injected embryos, nuclei reach the cortex in a timely fashion and continue to undergo cyclic rounds of division (though internuclear spacing during anaphase and telophase is abnormal; see also Zalokar and Erk, 1976). However, between cycles 10 and 13 many peripheral nuclei move away from the cortex and into the interior of the embryo (not shown), providing independent evidence that F-actin plays a role in holding microtubule arrays and nuclei at the cortex.

By cycle 12, the interphase distribution of cortical myosin II is restricted to the narrow base of the pseudocleavage furrows that separate closely packed buds. (see Fig. 6 in Field and Alberts, 1995). Because the heptane treatment that we use to remove oil and detach injected embryos glued to slides degrades the myosin-stainability of the cortex, we were unable to observe directly the effect mitotic cycle arrest or microtubule disruption has on cortical myosin II. However, time-lapse movies reveal that, in embryos stalled in a permanent interphase by cycloheximide, but in which colcemid has disrupted microtubules, disorganized, fast-moving, large-amplitude, convoluted, contractile waves develop and churn the entire cortex for hours (Fig. 10). Assuming these interphase contractions are actomyosin based, this rampant cortical contractility implies that, in the absence of microtubules, abundant myosin II must return to the cortex and co-localize with the F-actin that we detect there (Fig. 9C, upper panel). Nuclei dissociate from the writhing cortex and are displaced to a few microns beneath it (Fig. 9C, lower panel). This result

differs strikingly from what is observed in embryos arrested in metaphase by injection with just colcemid; our time-lapse recordings demonstrate that the cortex of cycle 12 and 13 embryos arrested in metaphase by an internal concentration of 100 μM colcemid remains mechanically quiescent for at least the two hours during which we normally film them (videos not shown).

We conclude from these drug injection experiments that: (1) the mechanism that removes F-actin from the cortex and concentrates it far beneath the cortex during interphase arrest must be microtubule-dependent (it fails when colcemid disrupts microtubules), (2) two completely different ways of eliminating F-actin from the cortex (by cytochalasin or by prolonging interphase and letting the microtubule-dependent mechanism strip off F-actin) cause nuclei to fall away from the cortex, but (3) the presence of F-actin alone at the cortex (without microtubules) is not sufficient to hold nuclei at the cortex, and (4) mitotic cycle phase affects cortex contractility, the cortex being actively contractile in interphase-arrested embryos, but inert in metaphase-arrested embryos.

DISCUSSION

We propose four high-level parsimonious hypotheses about mitotic-cycle-modulated interactions between the cell cortex *(*the approximately 3 μm deep zone immediately underlying the plasma membrane*)*, F-actin, myosin II, centrosomes and microtubules, which, working together, can explain our, and others', experimental results. These hypotheses imply no opinion about detailed molecular causes; interactions could be direct or caused by multipart complexes of auxiliary proteins. We state each hypothesis, connect it to our data, then cite literature providing supporting biochemical, genetic, or other data. We discuss cytokinesis studies because we propose an analogy between the cyclic cytoskeletal reorganizations that we observe in syncytial fly embryos, in which karyokinesis proceeds rapidly without cell division, and the way the mitotic apparatus locates the contractile ring during cytokinesis in typical mononucleate animal cells. We end by discussing how the mechanistic interactions that we hypothesize could generate the forces to protrude buds, to invaginate pseudocleavage furrows and to position cleavage furrows for standard cytokinesis.

Hypothesis H1: *mitotic phase modulates the amount of myosin II associated with the cortex and the amount of actin polymerized into filaments at the cortex; independent of the proximity of centrosomes and/or microtubules, both cortical myosin II and cortical F-actin increase from telophase through interphase then fall through metaphase and anaphase*

H1 simply summarizes the cyclic fluctuations in the cortical rim of high F-actin and myosin II concentration that we see in *Drosophila* embryos (Figs 1-5), which occur in both cycle 9 (microtubules absent) and cycle 10 (microtubules present). The surface views in Fig. 2 imply a dramatic temporal fluctuation in the total amount of cortical F-actin and myosin II staining, while Figs 1 and 3-5 show that F-actin and myosin II cyclically concentrate within ~3 μm of the cell surface.

H1 says the cortex is a diffusion trap that accumulates, and possibly stabilizes, myosin II filaments during one part of the mitotic cycle, from telophase to prophase. We lack a molecular understanding of how myosin II associates with the plasma membrane and how this localization is cyclically modulated. One component may be encoded by the gene *Drosophila lethal(2)giant larvae*, part of a multiprotein complex that associates tightly with plasma membrane and binds myosin II

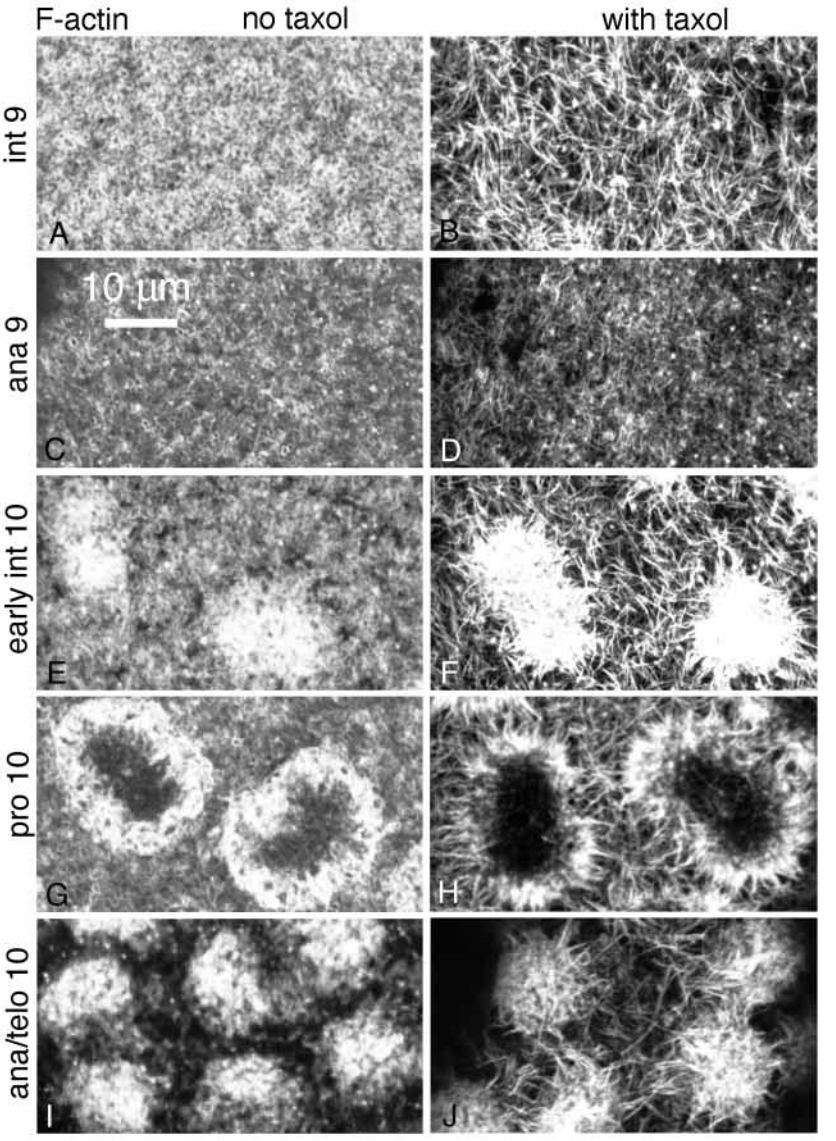

Fig. 7. Single section, surface view LSCM micrographs of cortical F-actin in (protocol 1) fixed phallicidin-stained embryos with (right column), and without (left column) a 1-1.5 minute taxol treatment. The fibers in the right column are *not* microtubules, but extraordinary F-actin structures induced by taxol-elicited extraordinary microtubules.

directly (Kalmes et al., 1996; Strand et al., 1994). The association between myosin and the *l(2)gl* protein is inhibited by phosphorylation (Kalmes et al., 1996), suggesting possible regulation via the $p34^{cdc2}$ kinase cascade. Alternately myosin's association with the actin-rich cortex may be controlled via phosphorylation of myosin itself. Studies on *Dictyostelium discoideum* show that phosphorylation of myosin heavy chain simultaneously determines myosin's assembly into bipolar filaments (Liang et al., 1999; Pasternak et al., 1989), the distribution of myosin between cortex and cytoplasm (Egelhoff et al., 1993; Yumura and Uyeda, 1997b), and in vivo actomyosin cortical contractility (Egelhoff et al., 1993).

H1 likewise says the cortex binds filamentous actin. We assume actin filaments are continually depolymerizing, so ongoing polymerization is needed to maintain equilibrium levels of F-actin; an increase in the rate of polymerization at one mitotic phase would yield higher levels of F-actin at that phase (assuming a constant depolymerization rate). We propose that, with no microtubules nearby (e.g. in cycle 9), the actin polymerization rate near the cortex is higher between telophase and prophase than during metaphase and anaphase. (Obviously an inverse variation of filament stability would accomplish the same result.) This same temporal modulation of actin polymerization rates must occur also in cycle 10 (and 11, etc), when centrosomes and microtubules immediately underlie the cortex, because it is obvious from inspection of rows 1-3 of Fig. 2 that there is no way to produce the caps of F-actin observed in early interphase 10 simply by redistributing the cortical F-actin pre-existing in anaphase 9. Whereas proteins that attach actin to plasma membranes are known (see for example Tsukita and Yonemura, 1997), cell cycle effects on these interactions are not yet known. From cycle 10 onward, cortical F-actin distribution is additionally influenced by nearby microtubule arrays, leading us to propose H2 and H3.

Hypothesis H2: *centrosomes, via the polymerization of the microtubule asters that they nucleate, boost the rate of actin polymerization nearby*

We hypothesize the elevation of actin polymerization rates near centrosomes to account for the genesis of the F-actin caps. In the *Drosophila* syncytium, cortical F-actin concentrations appear near centrosomes as the miniscule metaphase asters (Fig. 4) become extensive anaphase asters (Fig. 5). This occurs both when centrosomes are near the cortex (as shown here), or deep inside the embryo, as reported by von Dassow and Schubiger (1994).

How could centrosomes promote nearby actin polymerization during anaphase and telophase? Waterman-Storer and colleagues (1999) show that, in 3T3 fibroblasts, polymerization of microtubules activates Rac 1 GTPase, which in turn boosts actin polymerization. Neither the mere presence of stable microtubules, nor their depolymerization, has this effect. In the fly syncytial blastoderm at metaphase, few microtubules and only tiny asters at the spindle poles exist (Fig. 4). But during anaphase (Fig. 5), centrosomes nucleate large asters, which enlarge in telophase. If the mechanism that Waterman-Storer et al. (1999) discovered in 3T3 cells also operates in the fly embryos, then the large anaphase/telophase burst of centrosome-nucleated microtubule polymerization should cause a proportional increment in F-actin polymerization. Our 3-D reconstructions confirm that this burst of actin polymerization concentrates in the asters, near centrosomes (Fig. 5 rows 2 and 4). When centrosomes closely underlie the cortex (see Figs 1, 3-5), the Rac 1 mechanism of concentrating actin polymerization near centrosomes (H2) together with F-actin's increasing affinity for the cortex upon exit from mitosis (H1), could account for the formation of cortical F-actin caps shown in Figs 2-5. H2 could additionally account for the response to taxol that we observe. Brief treatment of permeabilized embryos with taxol causes a dramatic polymerization of haphazard microtubules just underlying the cortex and a concomitant change in cortical F-actin cortical organization (Fig. 7). Waterman-Storer et al. (1999) find that taxol treatment of 3T3 cells also promotes haphazard microtubule polymerization, which in turn causes a transient burst of actin polymerization.

The maternal-effect gene *mat(2)syn* ^{HK21} (Schupbach and Wieschaus, 1989), renamed *centrosomin* by Kaufman and coworkers, encodes a protein localized at centrosomes throughout syncytial blastoderm stages (Heuer et al., 1995; Li and Kaufman, 1996; Vaizel-Ohayon and Schejter, 1999). Homozygous *cnn*-defective mothers produce embryos with dramatic early defects in spindle organization, nuclear migration and pseudocleavage furrow formation. These embryos die without cellularizing (Li and Kaufman, 1996; Megraw et al., 1999; Vaizel-Ohayon and Schejter, 1999). Cnn protein, which is essential for normal centrosome assembly, also affects actin polymerization dynamics (Vaizel-Ohayon and Schejter, 1999). Although cortical F-actin in *cnn* mutant embryos is reportedly normal prior to nuclear arrival, when migrating nuclei reach the cortex, F-actin caps fail to form above them and pseudocleavage furrows fail to invaginate (Vaizel-Ohayon and Schejter, 1999); astral microtubule arrays form poorly or not at all, though functional spindles do form (Megraw et al., 1999; Vaizel-Ohayon and Schejter, 1999), apparently nucleated from chromosomes and assembled into spindles by motor proteins. These observations, like those of Waterman-Storer et al. (1999) implicate centrosome-nucleated microtubule dynamics in actin polymerization dynamics.

Hypothesis H3: *a kinesin-like activity attaches actin filaments to adjacent microtubules and transports actin filaments towards microtubule plus ends; this activity is weaker than the attachment of F-actin to the cortex*

This hypothesis accounts for effects microtubules have on reorganizing cytoplasmic F-actin three-dimensionally in the embryo interior and reorganizing cortical F-actin in the plane of the cortex. When microtubules lie close to, and tangent to, the cortex, this hypothesis implies plus end transport of cortex-bound filaments in the plane of the cortex, until continued transport along a microtubule would tear an actin filament away from the cortex. Then either the transport mechanism drags both the actin filament *and* the cortex that it is attached to towards the embryo's interior (as in pseudocleavage furrow invagination), or, if the membrane stays put, the kinesin motor stalls and the actin filament remains attached until depolymerization melts it.

Plus ends of elongating microtubules growing out from centrosomes, leaving a wake of activated Rac 1, leaving in turn a wake of actin polymerization (Waterman-Storer et al., 1999),

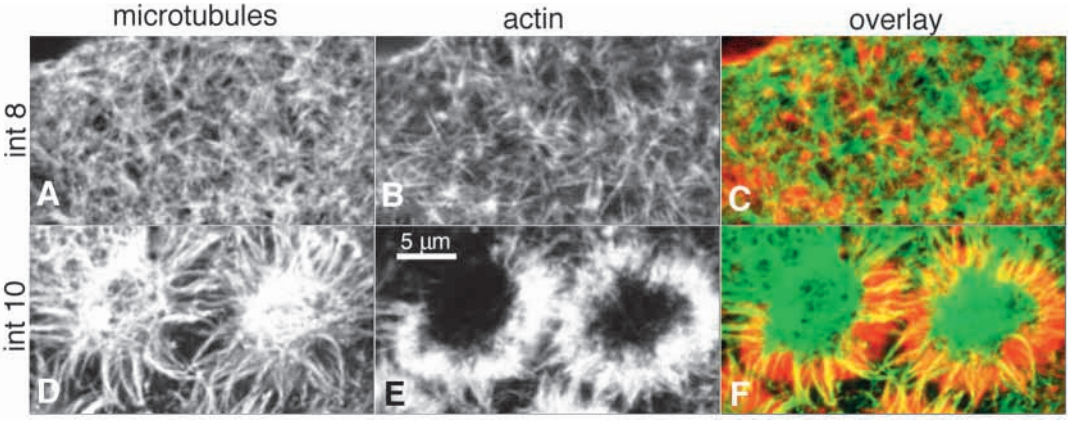

Fig. 8. Surface view LSCM micrographs of taxol-treated embryos, fixed by protocol 2 in interphase 8 (first row) and late interphase 10 (second row). The microtubules (left column, antibody labeled) are green in the right overlay column. Actin filaments (center column, phallicidin-labeled) are red in the overlays. Thus, yellow regions in the overlays mark the rare loci where microtubules and actin filaments coincide. With the notable exception of the 'tufts' at the edge of actin rings (see Results), the alignment of taxol-boosted microtubules and actin filaments appears no greater than random placement would produce.

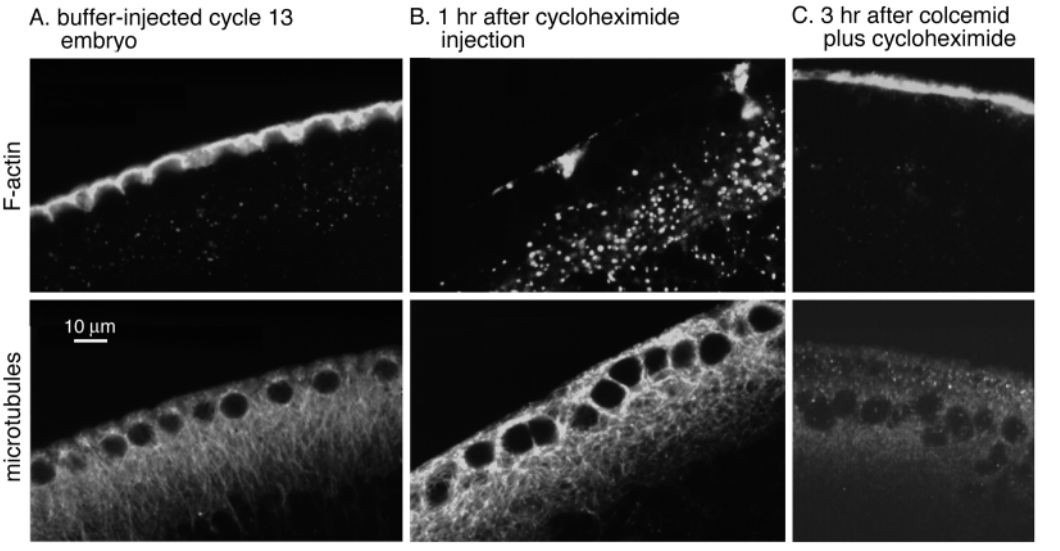

Fig. 9 F-actin (top row) and microtubules (bottom row) in fixed, stained cycle 13 embryos. Nuclei occupy unstained spheres in bottom panels. Column A is a buffer-injected control embryo. Column B is an embryo fixed 1 hour after injecting cycloheximide to 20 μg/ml. Column C is an embryo fixed 3 hours after injecting cycloheximide to 20 μg/ml plus colcemid to 100 μM. Imaging of F-actin and microtubules are as for Fig. 6.

could account for the formation of F-actin caps during anaphase through early interphase (Fig. 5, rows 2 and 4; Fig. 2, rows 3, 7 and 8). It will *not* explain, however, the subsequent hollowing out of F-actin caps into rings (Fig. 2, rows 3-5; Fig. 4, row 2) or account for the removal of F-actin from the cortex during a drug-prolonged interphase and its concentration near the plus ends of microtubules (Fig. 9B). The conversion of F-actin caps into hollow rings could result from nuclei pressing up into, and thereby excluding F-actin from the apices of buds. However, the equally common 'figure-of-eight' F-actin pattern observed overlying many prophase nuclei (with centrosomes at the center of each ring and a 'cross bar' of F-actin between the apical crown of the nuclear membrane and the plasma membrane – see right-most nuclei in row 5 of Fig. 2 and row 2 of Fig. 4) excludes this possible explanation. The gradual conversion of F-actin caps into hollow rings might arise simply because dense microtubule asters exclude F-actin. But the concentration of F-actin at the center of dense, assumed reversed-polarity microtubule asters (Fig. 6A), which polar body chromosomes nucleate and taxol amplifies, argues against that. However, movement of F-actin along centrosome-nucleated microtubules, towards microtubule plus ends, can simultaneously explain the prophase figure-of-eight F-actin patterns around separated individual centrosomes and F-actin rings encircling both centrosomes (eg. row 5 of Fig. 2). Cortical F-actin moving away from centrosomes is also consistent the accumulation of F-actin in the central core where the plus ends of microtubules of the reversed polarity aster converge (Fig. 6A), and the outcomes of our drug studies, discussed below. Fig. 11A,B cartoon the reorganizations of F-actin that hypothesis H3 would produce in centrosome-nucleated and reverse-polarity microtubule arrays, respectively.

The F-actin kinematics of Fig. 2, and everything just described in the previous paragraph, would result if something that promotes actin polymerization, rather than F-actin itself, associated with microtubules and continually moved along them toward microtubule plus ends. We favor the hypothesis that it is actin filaments that attach to and move along microtubules by some complex involving a kinesin because: (1) studies of cytokinesis in other model organisms have shown that, by *some* means, cortical flows of stabilized actin filaments do occur in vivo (Cao and Wang, 1990a,b); and (2) a beautiful in vitro study using cell-free lysates of *Xenopus* eggs showed that stabilized F-actin binds along the length of microtubules

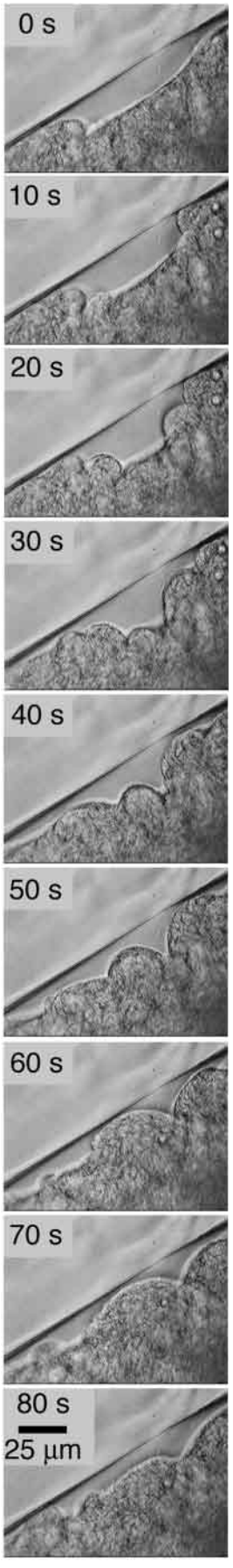

Fig. 10. Time-lapse movie frames of an embryo injected about 40 minutes previously in interphase 13 with cycloheximide (to interphase arrest) and colcemid (to disrupt microtubules). The frames, spaced at 10 second intervals, reveal the extreme cortical churning that this causes; it continues for hours. No such movements occur in wild-type embryos. The entire time-lapse video is called mvyFig10.mov at http://raven.zoology.washington.edu/downTheTubes/

nucleated from demembranated sperm (Sider et al., 1999). Sider et al. (1999) find that F-actin associates with microtubules in the presence of cell lysate, but not in its absence, implying the involvement of intermediary molecules. Moreover, the distribution of F-actin along microtubules changes with time: 5-minute-old asters contain more F-actin in the aster center than do 15-minute-old asters, which have relatively more F-actin at their distal (plus) ends, suggesting microtubule-based plus-end-directed transport at work. The co-localization of cortical actin with taxol-stabilized microtubules at the outer ragged edge of actin rings (Fig. 8D-F) is likewise consistent with this interpretation.

Another reason our data favors attachment of actin filaments to microtubules and transport along them is that the proposed mechanical attachment of F-actin to both cortex and microtubules has the side effect that F-actin would act as a ‘glue’ holding microtubule asters to the cortex, consistent with our drug studies. H3 implies that dissociating F-actin from the cortex would permit microtubule asters (and associated nuclei) to fall away from the cortex, as we observe after cytochalasin injections eliminate F-actin or after cycloheximide injection produces an interphase of such long duration that all F-actin is stripped from the cortex. After microinjection of both cycloheximide (to cause interphase arrest) and colcemid, the F-actin remains concentrated at the cortex, but cortical contractions nevertheless displace nuclei from the cortex (Fig. 9C-bottom panel), presumably because, when colcemid eliminates microtubules, it breaks one link in the cortex–F-actin–microtubule chain.

H3 also explains the result that most F-actin is removed from the cortex during the cycloheximide-induced hour-long arrest in interphase 13, and ends up concentrated basally where the plus ends of microtubules terminate (Fig. 9B). Continuous operation of H3 would establish a conveyor belt of F-actin motoring towards the plus ends of long microtubules. But why wouldn’t cortical attachments prevent removal of F-actin from the cortex? Because, we assume, individual actin filaments persist no longer than a couple of minutes before depolymerizing (Theriot and Mitchison, 1992). Actin repolymerizing near the cortex, but not close enough to attach to that cortex, can be carried into the embryo’s interior along microtubules. Actin transported in filamentous form to the basal ends of long microtubules can, upon depolymerization, diffuse back towards the cortex. We assume it takes 60-80 minutes of a drug-prolonged interphase for the H3 transport mechanism to win the race against diffusion of actin monomers back to the cortex and for all F-actin to be concentrated in the embryo interior. Thus H3 would not be expected to clear F-actin from the cortex in the normal short-duration syncytial interphases. In the cycloheximide-prolonged interphase experiment, immediately F-actin is depleted from the cortex and so eliminates the ‘actin glue effect’, microtubule asters and their nuclei start falling away from the cortex. Immediately microtubule arrays leave the F-actin-depleted cortex, F-actin begins reappearing in the patches that microtubules have vacated (Fig. 9B), demonstrating the cortex’s normal interphase ability to accumulate F-actin (H1) wherever F-actin is not being convected away by microtubules. In the dual cycloheximide/colcemid injection experiment, depolymerization of microtubules defeats the transport process, so F-actin remains at the cortex permanently (Fig. 9C).

von Dassow and Schubiger (1994) studying nuclear migration in early *Drosophila* embryos (cycles 4-6), before nuclei and microtubules make contact with the cortex, observed cyclic F-actin reorganization patterns consistent with H2-H3, but in the embryo interior. Particles of cytoplasmic F-actin accumulate near centrosomes in anaphase and telophase. As interphase progresses to prophase, F-actin particles accumulate in an enlarging halo around centrosomes with the center of the halo increasingly depleted of F-actin. Prolonging interphase by cycloheximide injection (an experiment analogous to that illustrated here in Fig. 9B) massively concentrates F-actin granules where the distal plus ends of microtubules from adjacent asters converge (presumably in antiparallel orientation; see Fig. 12C in von Dassow and Schubiger, 1994) and depletes the area around centrosomes/nuclei of F-actin. In cycloheximide-injected embryos, cytoplasmic F-actin re-localizes more rapidly than F-actin attached to the cortex (as the logic of the previous paragraph predicts), but both reorganizations are consistent with plus-end transport of F-actin along microtubules. Is there genetic evidence for a motor that (possibly indirectly) moves actin along astral microtubules towards their plus ends? We speculate that the essential kinesin-like protein PAV-KLP (homologue of mammalian *MKLP-1*), perhaps in association with Polo Kinase (Adams et al., 1998; Carmena et al., 1998; Nigg, 1998), may be such a motor.

Hypothesis H4: *a kinesin-like activity moves myosin II filaments towards microtubule plus ends; this is stronger than the attachment of myosin to the cell's cortex so that appropriately oriented microtubule arrays contacting the cortex strip myosin II off the plasma membrane*

Fig. 11 diagrams the effect centrosome-nucleated microtubule arrays and reversed-polarity polar body asters would have on myosin II, via H4. H4 accounts for why myosin II normally vacates regions of the cortex centered at centrosomes from which microtubules radiate (Figs 1-3) and likewise vacates regions where microtubule arrays nucleated from polar bodies contact the cortex (Fig. 6D). An alternative would be radiation, toward microtubule plus ends, of a signal that causes myosin II to release its attachment to the cortex, after which it just diffuses away. We prefer directed movement of myosin II along microtubules because that hypothesis, but not the alternate, can also explain myosin II relocalizations in *Dictyostelium discoideum* mutants (Yumura and Uyeda, 1997a; Zang and Spudich, 1998).

In *Dictyostelium* myosin mutants whose myosin heavy chains cannot be phosphorylated (and hence cannot be depolymerized), filaments of mutant myosin still localize normally to the contractile furrow during mitosis and to the tails of migrating interphase cells (Yumura and Uyeda, 1997b). Thus, in this lower eukaryote, myosin II thick filaments actually move rather than depolymerize at one site and re-polymerize elsewhere. It is also relevant that, in *Dictyostelium* cells null for the normal myosin II gene, three different mutant myosin II constructs move to the equator of dividing cells even though none of these three mutant constructs can hydrolyze ATP, or cause furrow constrictions (Yumura and Uyeda, 1997a). Likewise myosin II tails shorn of their actin-binding heads still aggregate to the cell equator in mitotic *Dictyostelium* cells null for normal myosin II, though the myosin tail polypeptide remains cytoplasmic and does not localize to the cleavage furrow cortex (Zang and Spudich, 1998). While neither research team tested whether myosin II localization requires microtubules, their data provide strong evidence that actomyosin contractility is not required to transport at least *cytoplasmic* myosin II to the cell equator, overturning a common assumption, and one consistent with H4. If myosin II translocation to the equator is occurring via microtubule transport, the finding that 'triple–ala' mutants (which mimic constitutive dephosphorylation) overaccumulate myosin at the contractile ring (Sabry et al., 1997) would then mean that, in *Dictyostelium*, it is probably only dephosphorylated myosin II heavy chain assembled into filaments that moves in this fashion.

If myosin II translocation occurs via microtubules, how might this occur? Recent work on unconventional (non-filament forming) myosins suggests a possible answer. Huang and coworkers have shown that a region in the tail of mammalian myosin VA, a two-headed myosin with actin-activated ATPase activity (Cheney et al., 1993), interacts with a roughly 100-amino-acid portion of the tail of conventional kinesin heavy chain (Huang et al., 1999). This interaction, identified using a yeast two-hybrid screen, is highly specific. Perhaps myosin II heavy chain likewise interacts via its tail directly or indirectly with a kinesin.

Mitotic effects on cortical contractility

We find that the cortex of *Drosophila* syncytial blastoderm embryos arrested in interphase (by cycloheximide injection) with microtubules depolymerized (by colcemid) is actively contractile (Fig. 10), whereas the cortex in embryos in metaphase arrest (by colcemid injection) is noncontractile. This matches studies of cortical contraction in frog blastomeres in which relaxation occurs in response to activated $p34^{cdc2}$, while contraction occurs upon $p34^{cdc2}$ inactivation (Rankin and Kirschner, 1997). In cycle 9 and 10 syncytial *Drosophila* embryos, we observe a decrease in myosin II (and F-actin) at the cortex during each metaphase and anaphase, then a rapid rise during telophase to a high level, which persists through interphase and prophase. Cyclic changes that simply determine whether F-actin and myosin co-localize at the cortex are potentially sufficient to explain our observed cyclic changes in cortical contractility. We do not know whether in higher eukaryotes myosin II is independently attached to the cortex (like actin) with this attachment subject to mitotic control, or whether myosin accumulates at the cortex via its interactions with actin, which interactions are mitotically controlled, or whether both types of regulation occur. Jordan and Karess (1997) find that, in *Drosophila*, oocyctes lacking myosin regulatory light chain (RLC) accumulate cytoplasmic aggregates of myosin heavy chain (among other abnormalities) hinting that RLC may affect myosin's ability to remain cortically bound. Perhaps RLC inhibitory sites ser-1 and ser-2, which $p34^{cdc2}$can phosphorylate (Pollard et al., 1990; Satterwhite et al., 1992; Yamakita et al., 1994), regulate cyclic changes in myosin's association with the cortex.

Some mechanical implications of our four hypothesized mechanisms, acting in concert

If true and phylogenetically general, the four processes that we

hypothesize would have multiple and far-reaching mechanical implications for cell morphogenesis, of which we now focus on two examples. The left side of Fig. 12 illustrates how the cytoskeletal interactions that we propose, acting in concert, might generate forces that would cause bud protrusion, and pseudocleavage furrow invagination in the syncytial *Drosophila* embryo. The righthand diagrams show how precisely the same interactions could position and time F-actin and myosin II assembly between bipolar microtubule arrays in preparation for cytokinesis.

Buds may form by a monopolar 'global contraction-polar relaxation' mechanism

Why do buds protrude from the embryo surface? At the *Drosophila* egg's anterior end, where space between the plasma membrane and vitelline shell accommodates protrusions, we believe three forces, all acting in the same direction, cause buds to protrude. The region of the membrane that must be stretched to form each bud overlies centrosomes, which is where F-actin caps form (H2) beginning during telophase (H1), latching the microtubule array to the cortex (H3). This is also the region of the cortex that myosin II vacates (H4) immediately the telophase nucleus contacts the cortex. Removal of myosin II presumably weakens the very region of the cortex that will erupt in the fashion of an aneurysm, and this weakening, an instance of polar relaxation, sets the stage for a combination of three different forces to generate the aneurysm. First, microtubules, growing into the interior of the egg, collide with yolk particles and push upon them, either via kinesin-based transport of yolk particles, or simply by a 'polymerization ram mechanism' (see Peskin et al., 1993). This, iterated in interphase of cycles 10-14, progressively packs all the yolk particles into the center region of the embryo. Inward forces by microtubules on yolk produce opposite and equal outward reaction forces on microtubules, which they transmit to the centrosomes. This push of the entire nucleus-centrosome-microtubule aster assembly outward is focused precisely on that area of the cortex weakened by microtubule-dependent depletion of myosin II. The second force is a subtle consequence of H3; a kinesin-like motor can drag an actin filament attached to the cortex toward the microtubule's plus end only by overcoming viscous drag forces resisting the sliding of the actin filament's attachment to the cortex. The resulting myriad equal-and-opposite reaction forces required by Newton's laws push the microtubules that contact cortical F-actin back toward the centrosomes. Before the membrane overlying the nucleus erupts outward, the astral microtubules radiating out from the centrosome, tangent to and just underlying the membrane, are like the spokes of an erect umbrella in which all the spokes are in compression pushing on the umbrella's central hub (the centrosome). This arrangement is prone to buckling outward (or inward). Once any other action initiates a slight outward protrusion of a bud, this mechanism amplifies it; the larger the diameter of the hollow actin rings surrounding centrosomes become (see rows 4 and 5 of Fig. 2), the more effective are the compressive forces on the microtubules underlying the membrane at causing outward buckling of the bud. The third force may result from an actomyosin contraction of the bands between buds where the F-actin and myosin II coexist. Seen at low magnification, these bands constitute a roughly hexagonal network of interconnected actomyosin strands, presumably capable of contracting during interphase, surrounding the egg's entire surface. Contraction of this net of strands would cause all of them to indent the cortex. But the constraint that the plasma membrane always encloses a constant volume means any indentations made in the membrane cause equal volume outward bulges.

Note that the depolymerization of all but spindle microtubules in metaphase eliminates the scaffolding through which the first two forces are transmitted. The third (contractile net) force is maximal in interphase but vanishes at anaphase due to the observed dissipation of the cortical F-actin and myosin II at anaphase (H1). Therefore, buds start collapsing at metaphase and become flat by anaphase, as observed (live sequences of bud formation and breakdown are shown in Fig. 4 of Foe and Alberts (1983) and at http://raven.zoology.washington.edu/downTheTubes/.

Buds trying to erupt where no space exists to accommodate them, invaginate pseudocleavage furrows instead

There exists no space between the plasma membrane and the vitelline shell across most of the egg's perimeter. In these regions, 'buds' still form – we believe by exactly the same mechanisms – but their formation involves invagination of 'pseudocleavage furrows' between nuclei rather than protrusion of buds containing nuclei. Mechanically, *viewed from a coordinate system attached to the centrosomes*, the two kinds of deformation of the membrane are congruent. The reason why these interactions would also cause cortical nuclei to rotate 90° with respect to the cortex between anaphase and telophase (Foe and Alberts, 1983), as diagrammed in Fig. 12, is explained in Foe et al. (1993). There we reviewed evidence for, and first explicitly hypothesized, F-actin-microtubule interactions via a kinesin intermediary. Note also that H1, in concert with H3 and H4, provide a mechanism for moving actomyosin rings along microtubules from their initial apical locations down to the basal ends of elongated nuclei during the 'slow phase' of cellularization in interphase 14. Fig. 8 in Foe et al. (1993) diagrams this.

Why would microtubule depolymerization unleash disorganized contractility in *Drosophila* embryos arrested in interphase?

H1 explains the cyclic appearance and disappearance of myosin II staining at the syncytial cortex, and H4 accounts for myosin II leaving the cortex where microtubule arrays contact the cortex. When cycloheximide causes an everlasting interphase 13 arrest and colcemid eliminates all microtubules during that interphase 13 arrest, rampant contractility is unleashed (Fig. 10). We interpret this to mean that continuing operation of just H1, in the absence of microtubules, fails to segregate F-actin and myosin II into the complementary localizations shown in row 3 of Fig. 1 and rows 3, 4, 5 and 8 of Fig. 2. Myosin returning to the cortex, and encountering there the spatially heterogeneous interphase distribution of F-actin (in caps or rings), will initiate strong cortical contraction instabilities that dramatically churn the embryo during the artificially prolonged interphase. Embryos arrested in metaphase would be expected to remain quiescent, as observed, because the cortex loses its associated myosin II during metaphase/anaphase (H1). Why doesn't co-localized

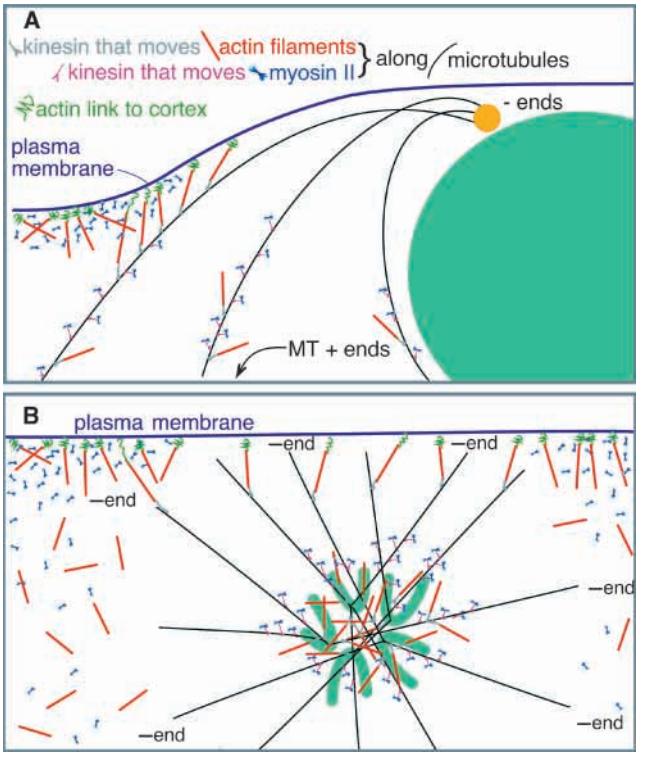

Fig. 11. Some consequences of hypotheses H1-H4 working in concert. Large green regions are chromatin, the orange circle is a centrosome. The top legend gives the rest of the colour/icon code. **(**A) A bud in late interphase. Concentrations of F-actin and myosin II begin at a uniform level across the cortex (H1), but, by late interphase, kinesin-mediated plus-end-directed transport along microtubules has swept both actin and myosin II filaments away from the centrosome. By H4, myosin II is stripped off regions of the cortex that microtubules contact. By H3, actin filaments can move no farther along microtubules than strong cortical attachment permits. This produces a snowdrift of actin filaments around the bud's perimeter. The stalled kinesins, trying to transport these actin filaments toward microtubule plus ends, 'glue' the microtubule aster to the cortex. Actin filaments that happen to form where they do not contact the cortex are dragged into the embryo's interior. (B) Our interpretation of Fig. 6. The plus ends of microtubules are in polar body kinetochore sockets so their minus ends face outward. Both F-actin (H3) and myosin II (H4) are cleared from the volume that the microtubule aster spans by plus-end-directed transport into the middle of the polar body cluster. Actin filaments attached both to the cortex and to a microtubule by a kinesin constitute a 'glue' holding, indeed pulling, the polar bodies to the cortex.

cortical F-actin and myosin II (as in row 1 of Fig. 1) destructively churn the embryo cortex during the interphase of cycle 9 and earlier, before migrating nuclei arrive? Firstly, before microtubule arrays contact the cortex in cycle 10, the interphase distributions of cortical F-actin and myosin II are globally uniform (cf. Fig. 2 row 2 versus rows 3-5) and, secondly, contractile instabilities take time to develop. Compared to the hours-long interphase that we effect by injecting cycloheximide, pre-cycle 10 interphases are very brief (<5 minutes at 25°C) and are interrupted by mitosis when cortical F-actin and myosin concentrations both plummet.

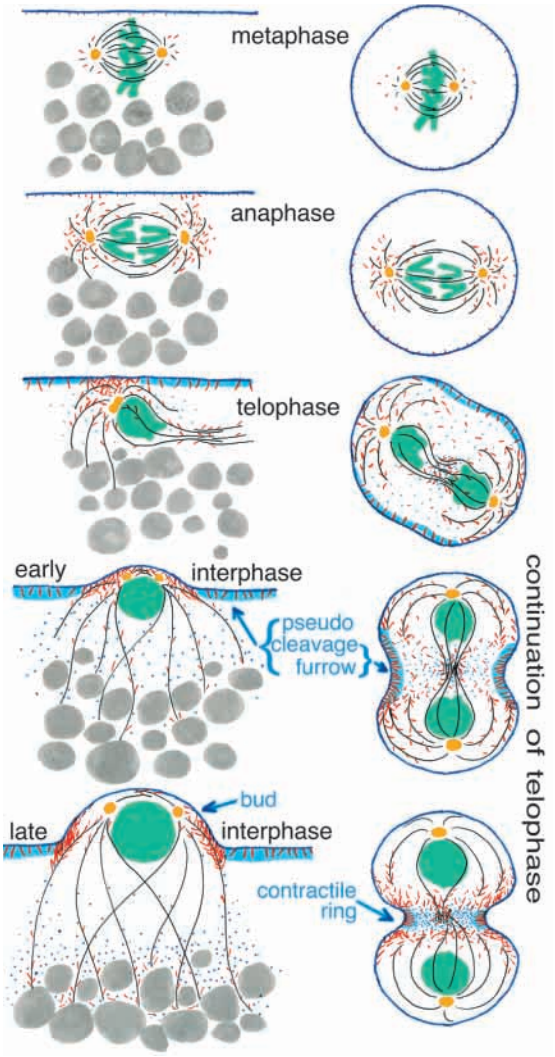

Fig. 12. Plasma membrane is dark blue, myosin II light blue, actin filaments red, microtubules black, centrosomes orange, chromatin green and yolk particles gray. Left column diagrams how the H1-H4 account for actin and myosin II kinematics produce budding cycles, from metaphase through late interphase, at the fly syncytial blastoderm's cortex (see Discussion). Compared to typical somatic cells, the centrosome division cycle is accelerated in early *Drosophila* embryos so that centrosomes duplicate in anaphase (Foe et al., 1993). The right column analogizes positioning and orientation of the contractile ring in preparation for cytokinesis in a large spherical mononucleate animal cell to *Drosophila* syncytial blastoderm events, assuming our four hypotheses operate in both. We rotated the cell on the left so one of its two nuclei has the same orientation as the single nucleus in the left column. We think it sensible to analogize an interphase phenomenon in the fly with a telophase phenomenon in a typical normal dividing cell because mitotic cycles proceed so rapidly in fly embryos that the entire telophase and interphase occur in the five minutes following the end of anaphase. In typical normal dividing animal cells, it takes at least this long for the mitotic apparatus to set up the contractile ring and furrow constriction to commence. The interactions between myosin II, F-actin and microtubules, if mediated by kinesin-like motors, will take a few minutes to redistribute the actomyosin machinery as seen in Fig. 2. In the fast-cycling fly syncytial blastoderm, interphase concludes during those few minutes; in the slower cell cycles typical of most animal cells, interphase is just beginning after those few minutes elapse.

In mononucleate cells, H1-H4 could localize actin and myosin to the spindle equator during telophase

The same four mechanical hypotheses that we propose to explain pseudocleavage furrow and bud formation in the fly syncytial blastoderm, *if* operative in dividing mononucleate cells, could time and initiate localization of the actomyosin components of the contractile ring for cytokinesis (cartooned in righthand panels of Fig. 12). H1, by melting down prior interphase F-actin structures during metaphase, and H2 by causing F-actin to re-polymerize near centrosomes beginning in anaphase, in effect force a redeployment of the cell's actin just prior to beginning the specialized task of cytokinesis. By H1, the cortical concentrations of F-actin and myosin II, having fallen to low concentrations in metaphase-anaphase, rebuild in telophase. But the expanding telophase microtubule asters approaching the cortex at opposite poles of the cell would trigger, via H4, depletion of *cortical* myosin II filaments near the spindle poles where microtubules impinge, while simultaneously concentrating myosin II filaments by moving them through the cytoplasm towards the cell mid-zone. H4 will thus eventually concentrate myosin II in a three-dimensional disk whose perimeter will become the contractile ring. By H2, actin polymer will form coincidentally with microtubule outgrowth initially most concentrated near centrosomes, followed later in telophase by a migration of F-actin along astral microtubules away from centrosomes (by H3) and toward concentration in a three-dimensional disk-shaped volume centered at the equator where it will co-localize with myosin II. The 'rings' of cortical F-actin seen in late interphase in Figs 2 and 3, and sketched in cross-sectional cartoons in the bottom left panel of Fig. 12 as cortical F-actin concentrations flanking the bud, correspond to where these equatorial disk volumes intersect the cortex in the dividing mononucleate cell – diagrammed in righthand panels of Fig. 12. The regions between buds in Figs 1 and 2, where both F-actin and myosin II are present *together* at the cortex during interphase (though concentrations of F-actin may be higher elsewhere) constitute the so-called pseudocleavage furrows in the fly syncytial blastoderm. In our view, this region would be homologous to the cortex of the cleavage furrow, which constricts during cytokinesis (cf. right and left panels in Fig. 12).

H1-H4 imply a bipolar 'global contraction-polar relaxation' mechanism for positioning the contractile apparatus for cytokinesis

Wolpert (1960) proposed that, in spherical cells, transient 'polar relaxation' would convert a global cortical contraction into a self-amplifying equatorial contraction. Computer simulations (White and Borisy, 1983) showed how contracting an initially isotropic actomyosin meshwork into an equatorial belt aligns the filaments parallel to the equator, as in a contractile ring, positioning them to cleave a cell in two by a purse-string contraction. Plus-end transport along astral microtubules of cortical F-actin (H3) and of myosin II filaments (H4) could provide a mechanistic explanation for this oft-hypothesized polar relaxation, while simultaneously causing an increase in equatorial tension (assuming that cortical contractile strength is proportional to co-localized F-actin and myosin II concentrations). The right side of Fig. 12 cartoons these reorganizations. Either polar relaxation, or equatorial strengthening, or both together, can set the stage for the kind of actomyosin contraction-based cytokinesis that Wolpert first proposed and Borisy and White modeled. Schroeder (1981) proposed that the establishment of the contractile furrow was actually a mechanism requiring two independent steps – the release in tension at the poles hypothesized by Wolpert, preceded by (or coincident with) a global increase in cortical tensioning. The global loss of actin and myosin from the cortex during metaphase/anaphase and their return beginning in telophase, which we observe in *Drosophila* embryos (H1), if phylogenetically general, could underlie the cyclic changes in cortical contractility emphasized by Shroeder (1981). Operating together, H1-H4 are potentially capable of implementing a 'global contraction-polar relaxation' mechanism of furrow initiation for cytokinesis. If cortical contractile strength is proportional to co-localized F-actin and myosin II concentrations, then H3 and H4 would bring about equatorial strengthening of the cortical actomyosin meshwork, in principal also implementing 'equatorial stimulation' (Rappaport, 1996). Note that, in flattened cells with small asters, the microtubules in the mid-zone between spindle poles are positioned to execute the same actomyosin rearrangements as astral microtubules in spherical cells (Wheatley and Wang, 1996). Note also that H3 plus H4 can cause equatorial concentration of whatever *cytoplasmic* actomyosin network a cell contains, focusing internal forces on the furrow cortex with the potential to aid furrow invagination in non-spherical cells. Homologies between cleavage and pseudocleavage while attractive come with the caveat that cortical tensioning (Schroeder, 1981) and microtubule outgrowth (see for example Henson et al., 1989) both occur earlier in the mitotic cycle during cytokinesis in echinoderms than during pseudocleavage furrow formation in *Drosophila* syncytia. We do not know the significance of this timing difference, and have initiated experiments in sand dollar embryos to explore whether the interactions that we detect in fly embryos are phylogenetically general.

In summary, our study has aimed to deduce, from descriptions of wild-type and drug-perturbed cytoskeletal kinematics of microtubules, F-actin and myosin II in syncytial *Drosophila* embryos, the specific ways that these filament systems must be interacting. The speculative mechanistic hypotheses we deduce, H1-H4, are consistent with a large body of circumstantial and partial evidence reviewed above. This machinery, if phylogenetically general, could unify old ideas about cytokinesis with new molecular findings, reconcile polar relaxation with equatorial stimulation models of furrow formation, and homologize cytoskeletal pseudocleavage furrow formation in syncytia with cleavage furrow formation in mononucleate cells. We anticipate exciting future revelations of the molecular details by which the products of an ensemble of key genes (e.g. *anillin*, *centrosomin*, *diaphanous*, *KLP-3A*, *pavarotti*, *polo kinase*, *Rac 1*, *septins*, etc.) collaborate to bring about and regulate the interactions between F-actin, myosin II, centrosomes and microtubules our studies imply.

V. E. Foe gratefully acknowledges fellowship support from the MacArthur Foundation without which this exploration of unorthodox ideas and large time investment in technique development would have been untenable. G. M. Odell and V. E. Foe thank the University of Washington's Royalty Recovery Fund for seed money grant RRF 65-2885. We thank Vera C. Foe for her interest and the gift of a fast computer at a crucial juncture; to her we dedicate this paper. C. M.

Field is supported by NIH GM 23928 awarded to T. J. Mitchison. For the generous gift of antibodies, we thank Michelle Moritz (for anti-gamma tubulin) and Daniel Kiehart (for anti-cytoplasmic myosin II). We thank George von Dassow, Eli Meir, Ed Munro, Jon Alberts, John Sisson and two anonymous reviewers for their many helpful comments on our manuscript.

REFERENCES

Adams, R. R., Tavares, A. A., Salzberg, A., Bellen, H. J. and Glover, D. M. (1998). pavarotti encodes a kinesin-like protein required to organize the central spindle and contractile ring for cytokinesis. *Genes Dev.* **15**, 1483-1494.

Afshar, K., Gish, B. and Wasserman, S. A. (1999). Functional characterization of the diaphanous formin homology protein during cell division and early development in Drosophila. *Molec. Biol. Cell* **10 Supplement**, 384a (Abstract 2222).

Baker, J., Theurkauf, W. E. and Schubiger, G. (1993). Dynamic changes in microtubule configuration correlate with nuclear migration in the preblastoderm Drosophila embryo. *J. Cell Biol.* **122**, 113-121.

Bonaccorsi, S., Giansanti, M. G. and Gatti, M. (1998). Spindle self-organization and cytokinesis during male meiosis in asterless mutants of Drosophila melanogaster. *J. Cell Biol.* **142**, 751-761.

Cao, L. and Wang, Y. (1990a). Mechanism of the formation of contractile ring in dividing cultured animal cells. I. Recruitment of preexisting actin filaments into the cleavage furrow. *J. Cell Biol.* **110**, 1089-1095.

Cao, L. and Wang, Y. (1990b). Mechanism of the formation of contractile ring in dividing cultured animal cells. II. Cortical movement of microinjected actin filaments. *J. Cell Biol.* **111**, 1905-1911.

Carmena, M., Riparbelli, M. G., Tavares, A. M., Adams, R., Callaini, G. and Glover, D. M. (1998). Drosophila polo kinase is required for cytokinesis. *J. Cell Biol.* **143**, 659-672.

Castrillon, D. H. and Wasserman, S. A. (1994). Diaphanous is required for cytokinesis in Drosophila and shares domains of similarity with the products of the limb deformity gene. *Development* **120**, 3367-3377.

Cheney, R. E., O'Shea, M. K., Heuser, J. E., Coelho, M. V., Wolenski, J. S., Espreafico, E. M., Forscher, P., Larson, R. E. and Mooseker, M. S. (1993). Brain myosin-V is a two-headed unconventional myosin with motor activity [see comments]. *Cell* **75**, 13-23.

Dan, K. (1954). The cortical movement in Arbacia punctulata eggs through cleavage cycles. *Embryologia* **2**, 115-122.

Egelhoff, T. T., Lee, R. J. and Spudich, J. A. (1993). Dictyostelium myosin heavy chain phosphorylation sites regulate myosin filament assembly and localization in vivo. *Cell* **75**, 363-371.

Field, C. M. and Alberts, B. A. (1995). Anillin, a contractile ring protein that cycles from the nucleus to the cell cortex. *J. Cell Biol.* **131**, 165-178.

Fishkind, D. J., Silverman, J. D. and Wang, Y. L. (1996). Function of spindle microtubules in directing cortical movement and actin filament organization in dividing cultured cells. *J. Cell Sci.* **109**, 2041-2051.

Foe, V. E. and Alberts, B. M. (1983). Studies of nuclear and cytoplasmic behaviour during the five mitotic cycles that precede gastrulation in Drosophila embryogenesis. *J. Cell Sci.* **61**, 31-70.

Foe, V. E. and Alberts, B. M. (1985). Reversible chromosome condensation induced in Drosophila embryos by anoxia: visualization of interphase nuclear organization. *J. Cell Biol.* **100**, 1623-1636.

Foe, V. E., Odell, G. M. and Edgar, B. A. (1993). Mitosis and morphogenesis in the Drosophila embryo: point and counterpoint. In *The Development of Drosophila*, vol. 1 (ed. M. Bate and A. Martinez Arias), pp. 149-300. Plainview, New York: Cold Spring Harbor Laboratory Press.

Hay, B., Jan, L. Y. and Jan, Y. N. (1988). A protein component of Drosophila polar granules is encoded by vasa and has extensive sequence similarity to ATP-dependent helicases. *Cell* **55**, 577-587.

Henson, J. H., Begg, D. A., Beaulieu, S. M., Fishkind, D. J., Bonder, E. M., Terasaki, M., Lebeche, D. and Kaminer, B. (1989). A calsequestrin-like protein in the endoplasmic reticulum of the sea urchin: localization and dynamics in the egg and first cell cycle embryo. *J. Cell Biol.* **109**, 149-161.

Heuer, J. G., Li, K. and Kaufman, T. C. (1995). The Drosophila homeotic target gene centrosomin (cnn) encodes a novel centrosomal protein with leucine zippers and maps to a genomic region required for midgut morphogenesis. *Development* **121**, 3861-3876.

Horwitz, S. B., Lothstein, L., Manfredi, J. J., Mellado, W., Parness, J., Roy, S. N., Schiff, P. B., Sorbara, L. and Zeheb, R. (1986). Taxol: mechanisms of action and resistance. *Ann. NY Acad. Sci.* **466**, 733-744.

Huang, J. D., Brady, S. T., Richards, B. W., Stenolen, D., Resau, J. H., Copeland, N. G. and Jenkins, N. A. (1999). Direct interaction of microtubule- and actin-based transport motors [see comments]. *Nature* **397**, 267-270.

Huynh, T. V., Young, R. A. and Davis, R. W. (1985). Constructing and screening CDNA libraries in lambda gt10 and lambda gt 11. In *DNA Cloning: A Practical Approach*, vol. 1 (ed. D. Glover), pp. 49-78. Oxford: IRL Press at Oxford University Press.

Jordan, P. and Karess, R. (1997). Myosin light chain-activating phosphorylation sites are required for oogenesis in Drosophila. *J. Cell Biol.* **139**, 1805-1819.

Kalmes, A., Merdes, G., Neumann, B., Strand, D. and Mechler, B. M. (1996). A serine-kinase associated with the p127-l(2)gl tumour suppressor of Drosophila may regulate the binding of p127 to nonmuscle myosin II heavy chain and the attachment of p127 to the plasma membrane. *J. Cell Sci.* **109**, 1359-1368.

Karr, T. L. and Alberts, B. M. (1986). Organization of the cytoskeleton in early Drosophila embryos. *J. Cell Biol.* **102**, 1494-1509.

Kellogg, D. R., Mitchison, T. J. and Alberts, B. M. (1988). Behavior of microtubules and actin filaments in living Drosophila embryos. *Development* **103**, 675-686.

Ketchum, A. S., Stewart, C. T., Stewart, M. and Kiehart, D. P. (1990). Complete sequence of the Drosophila nonmuscle myosin heavy-chain transcript: conserved sequences in the myosin tail and differential splicing in the 5' untranslated sequence. *Proc. Natl Acad. Sci. USA* **87**, 6316-6320.

Kiehart, D. P. and Feghali, R. (1986). Cytoplasmic myosin from Drosophila melanogaster. *J. Cell Biol.* **103**, 1517-1525.

Lajoie-Mazenc, I., Tollon, Y., Detraves, C., Julian, M., Moisand, A., Gueth-Hallonet, C., Debec, A., Salles-Passador, I., Puget, A., Mazarguil, H. et al. (1994). Recruitment of antigenic gamma-tubulin during mitosis in animal cells: presence of gamma-tubulin in the mitotic spindle. *J. Cell Sci.* **107**, 2825-2837.

Larabell, C. A., Rowning, B. A., Wells, J., Wu, M. and Gerhart, J. C. (1996). Confocal microscopy analysis of living Xenopus eggs and the mechanism of cortical rotation. *Development* **122**, 1281-1289.

Li, K. and Kaufman, T. C. (1996). The homeotic target gene centrosomin encodes an essential centrosomal component. *Cell* **85**, 585-596.

Liang, W., Warrick, H. M. and Spudich, J. A. (1999). A structural model for phosphorylation control of Dictyostelium myosin II thick filament assembly. *J. Cell Biol.* **147**, 1039-1048.

Mabuchi, I. (1986). Biochemical aspects of cytokinesis. *Int. Rev. Cytol.* **101**, 175-213.

Matthies, H. J., McDonald, H. B., Goldstein, L. S. and Theurkauf, W. E. (1996). Anastral meiotic spindle morphogenesis: role of the non-claret disjunctional kinesin-like protein. *J. Cell Biol.* **134**, 455-464.

Megraw, T. L., Li, K., Kao, L. R. and Kaufman, T. C. (1999). The centrosomin protein is required for centrosome assembly and function during cleavage in Drosophila. *Development* **126**, 2829-2839.

Miller, K. G., Field, C. M. and Alberts, B. M. (1989). Actin-binding proteins from Drosophila embryos: a complex network of interacting proteins detected by F-actin affinity chromatography. *J. Cell Biol.* **109**, 2963-2975.

Miller, K. G., Field, C. M., Alberts, B. M. and Kellogg, D. R. (1991). Use of actin filament and microtubule affinity chromatography to identify proteins that bind to the cytoskeleton. *Methods Enzymol.* **196**, 303-319.

Miller, K. G. and Kiehart, D. P. (1995). Fly division. *J. Cell Biol.* **131**, 1-5.

Neufeld, T. P. and Rubin, G. M. (1994). The Drosophila peanut gene is required for cytokinesis and encodes a protein similar to yeast putative bud neck filament proteins. *Cell* **77**, 371-379.

Nigg, E. A. (1998). Polo-like kinases: positive regulators of cell division from start to finish. *Curr. Opin. Cell Biol.* **10**, 776-783.

Pasternak, C., Flicker, P. F., Ravid, S. and Spudich, J. A. (1989). Intermolecular versus intramolecular interactions of Dictyostelium myosin: possible regulation by heavy chain phosphorylation. *J. Cell Biol.* **109**, 203-210.

Peskin, C. S., Odell, G. M. and Oster, G. F. (1993). Cellular motions and thermal fluctuations: the Brownian ratchet. *Biophys J.* **65**, 316-324.

Pollard, T. D., Satterwhite, L., Cisek, L., Corden, J., Sato, M. and Maupin, P. (1990). Actin and myosin biochemistry in relation to cytokinesis. *Ann. NY Acad. Sci.* **582**, 120-130.

Postner, M. A., Miller, K. G. and Wieschaus, E. F. (1992). Maternal effect mutations of the sponge locus affect actin cytoskeletal rearrangements in Drosophila melanogaster embryos. *J. Cell Biol.* **119**, 1205-1218.

Raff, J. W. and Glover, D. M. (1988). Nuclear and cytoplasmic mitotic cycles continue in Drosophila embryos in which DNA synthesis is inhibited with aphidicolin. *J. Cell Biol.* **107**, 2009-2019.

Rankin, S. and Kirschner, M. W. (1997). The surface contraction waves of Xenopus eggs reflect the metachronous cell-cycle state of the cytoplasm. *Curr. Biol.* **7**, 451-454.

Rappaport, R. (1996). *Cytokinesis in Animal Cells.* Cambridge, UK: Cambridge University Press.

Rothwell, W. F., Fogarty, P., Field, C. M. and Sullivan, W. (1998). Nuclear-fallout, a Drosophila protein that cycles from the cytoplasm to the centrosomes, regulates cortical microfilament organization. *Development* **125**, 1295-1303.

Sabry, J. H., Moores, S. L., Ryan, S., Zang, J. H. and Spudich, J. A. (1997). Myosin heavy chain phosphorylation sites regulate myosin localization during cytokinesis in live cells. *Mol. Biol. Cell* **8**, 2605-2615.

Satterwhite, L. L., Lohka, M. J., Wilson, K. L., Scherson, T. Y., Cisek, L. J., Corden, J. L. and Pollard, T. D. (1992). Phosphorylation of myosin-II regulatory light chain by cyclin-p34cdc2: a mechanism for the timing of cytokinesis. *J. Cell Biol.* **118**, 595-605.

Schejter, E. D. and Wieschaus, E. (1993). Functional elements of the cytoskeleton in the early Drosophila embryo. *Annu. Rev. Cell Biol.* **9**, 67-99.

Schroeder, T. E. (1981). The origin of cleavage forces in dividing eggs. A mechanism in two steps. *Exp. Cell Res.* **134**, 231-240.

Schupbach, T. and Wieschaus, E. (1989). Female sterile mutations on the second chromosome of Drosophila melanogaster. I. Maternal effect mutations. *Genetics* **121**, 101-117.

Sider, J. R., Mandato, C. A., Weber, K. L., Zandy, A. J., Beach, D., Finst, R. J., Skoble, J. and Bement, W. M. (1999). Direct observation of microtubule-f-actin interaction in cell free lysates. *J. Cell Sci.* **112**, 1947-1956.

Smith, D. B. and Johnson, K. S. (1988). Single-step purification of polypeptides expressed in Escherichia coli as fusions with glutathione S-transferase. *Gene* **67**, 31-40.

Strand, D., Jakobs, R., Merdes, G., Neumann, B., Kalmes, A., Heid, H. W., Husmann, I. and Mechler, B. M. (1994). The Drosophila lethal(2)giant larvae tumor suppressor protein forms homo-oligomers and is associated with nonmuscle myosin II heavy chain. *J. Cell Biol.* **127**, 1361-1373.

Sullivan, W., Minden, J. S. and Alberts, B. M. (1990). daughterless-abo-like, a Drosophila maternal-effect mutation that exhibits abnormal centrosome separation during the late blastoderm divisions. *Development* **110**, 311-323.

Theriot, J. A. and Mitchison, T. J. (1992). Comparison of actin and cell surface dynamics in motile fibroblasts. *J. Cell Biol.* **119**, 367-377.

Tsukita, S. and Yonemura, S. (1997). ERM proteins: head-to-tail regulation of actin-plasma membrane interaction. *Trends Biochem. Sci.* **22**, 53-58.

Vaizel-Ohayon, D. and Schejter, E. D. (1999). Mutations in centrosomin reveal requirements for centrosomal function during early Drosophila embryogenesis. *Curr. Biol.* **9**, 889-898.

Vincent, J. P. and Gerhart, J. C. (1987). Subcortical rotation in Xenopus eggs: an early step in embryonic axis specification. *Dev. Biol.* **123**, 526-539.

von Dassow, G. and Schubiger, G. (1994). How an actin network might cause fountain streaming and nuclear migration in the syncytial Drosophila embryo [published erratum appears in J. Cell Biol. 1995 Sep;130(5):1231-4]. *J. Cell Biol.* **127**, 1637-1653.

Wang, Y., Silverman, J. D. and Cao, L. (1994). Single particle tracking of surface receptor movement during cell division. *J. Cell Biol.* **127**, 963-971.

Warn, R. M., Magrath, R. and Webb, S. (1984). Distribution of F-actin during cleavage of the Drosophila syncytial blastoderm. *J. Cell Biol.* **98**, 156-162.

Waterman-Storer, C. M. and Salmon, E. (1999). Positive feedback interactions between microtubule and actin dynamics during cell motility. *Curr. Opin. Cell Biol.* **11**, 61-67.

Waterman-Storer, C. M., Worthylake, R. A., Liu, B. P., Burridge, K. and Salmon, E. D. (1999). Microtubule growth activates Rac 1 to promote lamellipodial protrusion in fibroblasts. *Nature Cell Biology* **1**, 45-50.

Wheatley, S. P. and Wang, Y. (1996). Midzone microtubule bundles are continuously required for cytokinesis in cultured epithelial cells. *J. Cell Biol.* **135**, 981-989.

White, J. G. and Borisy, G. G. (1983). On the mechanisms of cytokinesis in animal cells. *J. Theor. Biol.* **101**, 289-316.

Wolpert, L. (1960). The mechanics and mechanism of cleavage. *Int. Rev. Cytol.* **10**, 163-216.

Yamakita, Y., Yamashiro, S. and Matsumura, F. (1994). In vivo phosphorylation of regulatory light chain of myosin II during mitosis of cultured cells. *J. Cell Biol.* **124**, 129-137.

Yasuda, G. K., Baker, J. and Schubiger, G. (1991). Independent roles of centrosomes and DNA in organizing the Drosophila cytoskeleton. *Development* **111**, 379-391.

Yumura, S. and Uyeda, T. Q. (1997a). Transport of myosin II to the equatorial region without its own motor activity in mitotic *Dictyostelium* cells. *Mol. Biol. Cell* **8**, 2089-2099.

Yumura, S. and Uyeda, T. Q. (1997b). Myosin II can be localized to the cleavage furrow and to the posterior region of Dictyostelium amoebae without control by phosphorylation of myosin heavy and light chains. *Cell Motil. Cytoskeleton* **36**, 313-322.

Zalokar, M. and Erk, I. (1976). Division and migration of nuclei during early embryogenesis of Drosophila melanogaster. *J. Microbiol. Cell.* **25**, 97-106.

Zang, J. H. and Spudich, J. A. (1998). Myosin II localization during cytokinesis occurs by a mechanism that does not require its motor domain. *Proc. Natl. Acad. Sci. USA* **95**, 13652-13657.